NASA Contractor Report 181811

ICASE REPORT NO. 89-15

ICASE

NON-LINEAR EVOLUTION OF A SECOND MODE WAVE IN SUPERSONIC BOUNDARY LAYERS

Gordon Erlebacher

M. Y. Hussaini

Contract No. NAS1-18605

February 1989

INSTITUTE FOR COMPUTER APPLICATIONS IN SCIENCE AND ENGINEERING
NASA Langley Research Center, Hampton, Virginia 23665

Operated by the Universities Space Research Association

National Aeronautics and
Space Administration

Langley Research Center
Hampton, Virginia 23665

Non Linear Evolution of a Second Mode Wave in Supersonic Boundary Layers

Gordon Erlebacher
NASA Langley Research Center

M. Y. Hussaini*
Institute for Computer Applications in Science and Engineering

The non-linear time evolution of a second mode instability in a Mach 4.5 wall-bounded flow is computed by solving the full compressible, time-dependent Navier-Stokes equations. High accuracy is achieved by using a Fourier-Chebyshev collocation algorithm. Primarily inviscid in nature, second modes are characterized by high frequency and high growth rates compared to first modes. Time evolution of growth rate as a function of distance from the plate suggests this problem is amenable to the Stuart-Watson perturbation theory as generalized by Herbert.

* Research supported by the National Aeronautics and Space Administration under contract No. NAS1-18605 while resident at the Institute for Computer Applications in Science and Engineering (ICASE), NASA Langley Research Center, Hampton, VA 23665.

I. Introduction

Recent advances in supersonic and hypersonic aerospace technology have led to a renewed interest in the stability and transition to turbulence of high speed flows. The last 30 years have intermittedly witnessed some vigorous attempts to understand some of the fundamental routes to transition for incompressible flows. While a fairly comprehensive picture of the initial stages leading to the breakdown of an incompressible laminar boundary layer has emerged (mostly under controlled conditions) [9], the non-linear effects responsible for transition at high speeds are still very much a mystery. However, the current nonlinear incompressible theories, numerical simulations and experiments will, hopefully, serve as a guide in gaining a better understanding of the mechanisms present in the supersonic and hypersonic regimes.

Lees and Lin [13] were the first to study the linear stability of inviscid compressible flows in the 1940's. Their study was restricted to low Mach numbers and the conclusions drawn only apply to the first unstable mode. Mack unraveled some of the intricacies among the many possible modes present when the full stability equations are considered (including viscous and conductivity terms). From 1960 to the present time, Mack has devoted his energies to a thorough numerical investigation of the linear stability characteristics of inviscid compressible flows at both subsonic and supersonic Mach numbers. An extensive review of compressible linear theory appears in his 1984 AGARD report [16]. His research led to the discovery of the higher unstable modes for Mach numbers above 2.2. The importance of the higher modes stems from their high spatial and temporal amplification rates which make them susceptible to noise from the free-stream or from windtunnel walls. One of the main differences between first and second mode waves is their response to cooling. Wall cooling stabilizes first mode perturbation waves, while second mode perturbations are destabilized. At Mach numbers greater than 7, cone experiments have confirmed that the second mode is primarily responsible for the observed instabilities [22,3]. Therefore, new techniques must be developed to control the growth rates in these regimes.

The existence of an inflectional point in the mean boundary layer profile, a necessary and sufficient condition to insure the instability of inviscid incompressible flows, remains valid at all Mach numbers if the relative Mach number is subsonic everywhere [†]. For compressible flows, the inflection point is replaced by the generalized inflection point which takes into account the mean density variation across the boundary-layer. However, there are also non-inflectional waves which depend on the existence of local pockets of supersonic relative Mach number in the boundary-layer. These waves can be unstable and can exist at all supersonic free-stream Mach numbers. Multiple modes also exist for these non-inflectional waves. The above linear stability characteristics of compressible flows are fully described in Mack's review articles [16,17].

[†]The relative Mach number measures the difference between the mean velocity in the direction of the wave vector and the phase velocity with respect to the sound speed.

To date, there are only a handful of experiments that have studied the detailed linear stability characteristics of flat plates [12] and cones [10]. Laufer and Vrebalovich studied the linear stability of a Mach 2.2 flow on a flat plate, and theirs is perhaps the most complete (if not the only) flat plate experiment to date at supersonic velocities. Not only are hot wire measurements difficult to perform and to interpret correctly [19], but the stability characteristics of the boundary layer are affected by free-stream disturbances emanating from the wind tunnel walls. Since the disturbances scale as M_∞^2, it becomes increasingly difficult to obtain good, quantitative data at the higher speeds. The quiet Mach 6 tunnel, currently under construction at NASA Langley Research Center [1] should alleviate some of these concerns.

Among the few numerical codes geared towards the analysis of compressible stability, the best known are perhaps those of Mack [15] and Malik [18]. The former calculates spatial and temporal amplification rates, while the latter is strictly restricted to temporal analysis; a Gaster transformation is then applied to calculate the temporal and spatial growth rates. A new spectral stability code has also been developed at NASA Langley [14]. Until the work by Erlebacher and Hussaini [6,7], there have been no non-linear simulations. Erlebacher and Hussaini studied the evolution of two 3-D waves superimposed on a 2-D wave. These were first mode waves. They numerically demonstrated the existence of a secondary instability at Mach 4.5. The current incompressible weakly non-linear theory of Herbert [8] has been extended to include compressible flow by El-Hady [4] and Nayfeh [20]. Nayfeh treats both subsonic and supersonic regimes, while El-Hady only presents results up to Mach 1.2. Both studies are based on a quasi-parallel theory and treat subharmonic disturbances.

In this paper, a recent code developed to solve numerically the non-stationary, three-dimensional compressible Navier-Stokes equations applied to wall-bounded flows, is used to study the nonlinear evolution of one two-dimensional second mode at Mach 4.5. A possible application of perturbation analysis to this problem is also discussed.

II. Equations

The compressible Navier-Stokes equations for the stability of parallel flows are, in dimensionless form, (Erlebacher and Hussaini [6])

$$\frac{\partial \rho}{\partial t} + \nabla\cdot(\rho\vec{v}) = 0 \tag{1}$$

$$\frac{\partial(\rho\vec{v})}{\partial t} + \nabla\cdot(\rho\vec{v}\vec{v}) = -\nabla p \frac{1}{Re}\nabla\cdot\vec{\vec{\tau}} \tag{2}$$

$$\frac{\partial p}{\partial t} + \vec{v}\cdot\nabla p + \gamma p \nabla\cdot\vec{v} = \frac{1}{RePrM_\infty^2}\nabla\cdot(\mu\nabla T) + (\gamma-1)\Phi \tag{3}$$

where

$$\vec{\vec{\tau}} = \mu(\nabla\vec{v} + \nabla\vec{v}^T) - \frac{2}{3}\mu(\nabla\cdot\vec{v})\,\vec{\vec{I}} \tag{4}$$

is the viscous stress and

$$\Phi = \frac{1}{2}(\nabla\vec{v} + \nabla\vec{v}^T) : \vec{\tau} \tag{5}$$

is the viscous dissipation function. The equation of state is

$$\gamma M_\infty^2 p = \rho T, \tag{6}$$

with $\gamma = C_p/C_v$, the ratio of specific heats. At high Mach number, temperature variations across the boundary layer become important and the temperature dependence of viscosity must be taken into account. The Prandtl number is assumed equal to 0.7, and Sutherland's law is prescribed for viscosity. Lengths are non-dimensionalized with respect to the displacement thickness δ^*. Velocity, temperature, viscosity, and density are normalized with respect to free-stream values. Pressure is normalized with respect to the total head $\rho_\infty U_\infty^2$.

In incompressible boundary-layer flows, it has been observed that the evolution to laminar breakdown for ribbon-excited Tollmien-Schlichting (TS) waves occupies a space of several TS wavelengths [11]. Apart from numerical considerations, a direct simulation of a 3-D boundary layer flow far into the non-linear regime is not currently practical, even on today's most powerful computers. The situation is worse for compressible flows where the instability mechanisms are attenuated. One possible approximation is to neglect the growth of the mean boundary-layer. The perturbation flow is then periodic and the expense of the simulation is greatly decreased. This has been successful in incompressible theories [8] and numerical simulations [24]. One of the major reasons for this success is that the actual transition process occurs within a very short streamwise extent. At high Mach numbers, the growth rates are attenuated, the transition region is longer, and it is not clear whether this approximation is valid. Nonetheless, in an initial attempt to gain insight into the physics of second mode wave evolution, a temporal simulation is considered. The hope is that the observed features are at least qualitatively correct. The computational domain is restricted to one period in the streamwise distance. Periodicity is also assumed in the spanwise direction. A properly posed initial-value problem is set up, and qualitative comparisons are made with experimental data by relating time (in the simulations) to the streamwise direction (x) in the experiments. In order that the mean parallel boundary layer flow, $(\rho_m(y), U_m(y), T_m(y))$, be a stationary solution to the Navier-Stokes equations, source terms must be added to equations (2)-(3). The x momentum equation must be supplemented by the term

$$\mathcal{F}_{\rho u} = \frac{1}{Re}\frac{\partial}{\partial y}\left(\mu\frac{\partial U_m}{\partial y}\right) \tag{7}$$

while the forcing term

$$\mathcal{F}_p = \frac{1}{RePrM_\infty^2}\frac{\partial}{\partial y}\left(\mu\frac{\partial T_m}{\partial y}\right) + \frac{1}{Re}\left[\left(\frac{\partial U_m^2}{\partial y}\right)^2\right] \tag{8}$$

must be added to the energy equation (3). In obtaining these relations, the mean pressure is kept constant across the boundary layer. The mean velocity has only a streamwise component.

III. Algorithm

The algorithm described below, has been implemented in 3-D although only 2-D results are presented in this paper. Three-dimensional simulations of first mode wave interactions have been detailed elsewhere [7]. The system of equations (1) -(3) is solved in conservative form under the parallel flow assumption. Periodic boundary conditions in the streamwise and spanwise directions permit a Fourier representation of the primitive variables $\vec{v}$, p and ρ. For example,

$$\vec{v}(x,y,z,t) = \sum_{k=-N_x/2+1}^{N_x/2} \sum_{l=-N_z/2+1}^{N_z/2} \hat{\vec{v}}(y,t)\, e^{\imath(\alpha k x + \beta l z)} \tag{9}$$

where N_x, N_z are the number of collocation points in the streamwise and spanwise directions, and α, β are the wavenumbers in these same two directions. The periods of the physical domain in the streamwise and spanwise directions are respectively $2\pi/\alpha$ and $2\pi/\beta$. In the absence of discontinuities in the solution, spectral collocation methods offer a high degree of accuracy and minimum dispersion and dissipation errors. Periodicity in the two horizontal directions allows the use of Fourier collocation methods. In the direction normal to the plate, Chebyshev collocation is the natural choice. The physical domain $y \in [0, y_{max}]$ in the direction normal to the plate is mapped onto the computational domain $\eta \in [-1, 1]$ through a convolution of two mappings. First, a hyperbolic tangent transformation takes η to an intermediate variable ψ according to

$$\psi + t_\epsilon \tanh\left(\frac{\psi - \psi_0}{\Delta\psi}\right) = \frac{\eta - \eta_0}{\Delta\eta}. \tag{10}$$

In this equation, the hyperbolic tangent concentrates nodes about ψ_0, and $\Delta\psi$ measures the width of the concentration region. t_ϵ measures the degree of influence of the hyperbolic tangent term. If $t_\epsilon = 0$, there is no redistribution of nodes at this level. An algebraic stretching then maps ψ onto the physical variable $y \in [0, y_{max}]$. This mapping takes the form

$$y = \frac{y_{1/2} y_{max}(1+\psi)}{y_{max} - \psi(y_{max} - 2y_{1/2})} \tag{11}$$

One half the normal nodes are located between $y = 0$ and $y = y_{1/2}$. With both mappings in hand, $\eta_0, \Delta\eta$ ψ_0 and $\Delta\psi$ are readily determined. The user specifies the following: 1) t_ϵ, 2) y_0, the physical location about which the concentration occurs, 3) Δy_0, the concentration width in physical space, 4) y_{max}, the maximum vertical extent of the physical domain, and 5) $y_{1/2}$. Admittedly, the selection is rather tedious, but it is only executed once to optimize the distribution of nodes relative to the initial perturbation wave profiles. The distribution of nodes is fixed during the simulation. Δy_0 and $\Delta\psi$ are related via

$$\Delta\psi = \left.\frac{d\psi}{dy}\right|_{y=y_0} \Delta y_0 \tag{12}$$

while ψ_0 is computed from the algebraic mapping evaluated at y_0. The two remaining unknowns, η_0 and $\Delta\eta$ follow from the conditions

$$\eta(\psi)|_{\psi=-1} = -1$$

$$\eta(\psi)|_{\psi=+1} = +1 \tag{13}$$

which leads to

$$\begin{aligned} \Delta\eta &= \frac{2}{2 + t_\epsilon(T_- + T_+)} \\ \eta_0 &= \frac{t_\epsilon(T_+ - T_-)}{2 + t_\epsilon(T_- + T_+)} \end{aligned} \tag{14}$$

where

$$T_\pm = \tanh\left(\frac{1 \pm \psi_0}{\Delta\psi}\right) \tag{15}$$

All runs were performed with $y_{max} = 15$, $y_{1/2} = 1$, $t_\epsilon = 0.8$, $y_0 = 1.2$ and $\Delta y_0 = 0.4$.

IV. Initial and Boundary Conditions

In this paper, only the evolution of 2 dimensional waves are considered. Therefore, the initial conditions consist of a 2-D waves superimposed on a precalculated mean flow. Mean flow profiles are generated from the spectral solution to the similar compressible boundary-layer equations with zero pressure gradient and zero heat transfer at the wall [6], while the perturbation wave is a two-dimensional eigenfunction of the linearized compressible Navier-Stokes equations. The stability of flows is studied at a prescribed supercritical Reynolds number $Re(x_0)$. After freezing the streamwise dependence of the mean flow profiles at $x = x_0$, they are extended over the entire plate. Thus, the displacement thickness is constant, and the mean flow is a function only of the coordinate normal to the plate.

The initial condition for u(x,y,z) is therefore

$$u(x, y, z) = u_m(y) + \epsilon_{2D} u_{2D}(y) \cos(\theta_{2D}(y) + \alpha x) \tag{16}$$

with similar relations for the remaining 4 variables (v, w, p, ρ). The 2-D wave is an eigenfunction to the linearized Navier-Stokes equations and is calculated with the spectral linear compressible stability code SPECLS [14]. The angle θ_{2D} is the phase angle of the complex TS wave. The amplitudes u_{2D} is normalized to unity. Therefore, ϵ_{2D} is the amplitude of the two-dimensional perturbation wave with respect to the free-stream velocity. At high Mach numbers, ϵ_{2D} cannot exceed a couple of percent lest the density and temperature maxima (which scale as M_∞^2) become excessive.

Under the assumption of parallel flow, all the variables are periodic in the streamwise and spanwise directions. No-slip conditions are applied to the velocities at the wall which is adiabatic. In the far-field, the variables are either frozen at their initial values (which are vanishingly small) or calculated from zero stress conditions. These approaches both preclude the study of boundary-layer receptivity to incoming sound waves. The frozen boundary conditions also prevent waves from escaping into the free-stream. When the

far-field boundary is sufficiently removed from the wall, stability mechanisms which do not involve far-field interactions can still be successfully analyzed.

Zero normal stress boundary conditions lead to an exponential decay of the solution in the free-stream, but not at the proper rate. However, it is plausible that the feedback from the free-stream into the interior of the domain is not as severe as for the frozen far-field conditions. These boundary conditions are derived from a variational formulation of the Navier-Stokes equations. The velocities and temperature are assumed to possess C^1 continuity, while the pressure is only required to be C^0. The natural boundary conditions of this formulation in the far-field are then [21]

$$w_x + u_z = 0 \tag{17}$$

$$w_y + v_z = 0 \tag{18}$$

$$-pRe + 2w_z + \lambda(u_x + v_y + w_z) = 0 \tag{19}$$

$$pw = \frac{1}{\gamma PrReM_\infty^2}(\mu \frac{\partial T}{\partial z}) \tag{20}$$

If $(\tilde{u}, \tilde{v}, \tilde{w}, \tilde{p}, \tilde{T})$ are deviations of (u, v, w, p, T) from free-stream values, the resulting linearized equations become

$$\tilde{u}_z - \iota\alpha\tilde{w} = 0 \tag{21}$$

$$\tilde{v}_z - \iota\beta\tilde{w} = 0 \tag{22}$$

$$-\tilde{p}Re + (2+\lambda)w_z + \lambda(\iota\alpha u + \iota\beta v) = 0 \tag{23}$$

$$\tilde{w} - \frac{1}{\gamma PrReM_\infty^2}T_z = 0 \tag{24}$$

$$\gamma M_\infty^2 \tilde{p}_z - \tilde{\rho}_z + \tilde{T}_z = 0. \tag{25}$$

Derivatives in the vertical direction are evaluated using matrix multiplication. In this way, the unknowns (primitive variables at the last node) can be solved for simultaneously. The alternative are FFT's, which lead to an iterative approach. The interior nodes have already been computed from the explicit time advancement. Therefore, the derivative of u at the far field (node N) is represented by

$$\left.\frac{du}{dy}\right|_{y=y_1} = \sum_{i=1}^{N} D_{ij}u_j \tag{26}$$

where D_{ij} is the collocation derivative matrix [2] and where the only unknown is u_N. The system of equations (21)-(25) reduces to a linear system for the unknowns (u_N, v_N, w_N, T_N). Density has already been calculated through the continuity equation imposed at the outer boundary. A disadvantage comes from the higher truncation errors associated with matrix multiplication when compared to FFT's for large number of collocation points. There are at least two remedies. First, an implicit, rather than an explicit time advancement scheme could incorporate these asymptotic boundary-conditions into the iterative inversion scheme. This could be done solely with FFT's. The second approach is to adopt

a multidomain decomposition in the direction normal to the plate. An explicit scheme still requires matrix multiplication for derivative evaluation, but the number of nodes in each subdomain is small, and truncation errors will not affect the numerical results as strongly as in the single domain case. As the Mach number increases, the structure of the perturbation waves is mostly due to the density in a thin region centered about the critical layer whose distance away from the wall is approximately constant in terms of δ^*. Boundary conditions at the interface between two domains of a multidomain methods are continuity of all primitive variables (in the absence of shocks) and zero normal stress across the interface. A condition similar to zero normal stress can be derived from the energy equation. For best results, the interface conditions should be derived from the actual set of equations solved in the simulation. As yet, the multi-domain approach has not been implemented into the code. A more detailed description of this approach will be given elsewhere. All results presented below are based on the zero stress far-field conditions.

V. Cost of Direct Simulation

Timings on the Cray 2 at NASA Ames indicate that one iteration of the compressible Navier-Stokes equations is approximately twice the cost of one iteration of an incompressible spectral Navier-Stokes code. However, the ratio is actually higher for a given amplification factor for the following reasons. Although the high Mach number regime does not require an implicit treatment of the acoustic terms, grid refinement in the vertical direction in the course of the simulation imposes a severe time step constraint due to the viscous terms. In the absence of grid stretching, a Chebyshev collocation method imposes a maximum explicit time step that scales as N^{-4}, where N is the number of collocation points. With an algebraic grid stretching, points are more sparse in the free-stream, but concentrated at the origin, which decreases the time step further. Fortunately the hyperbolic tangent stretching, which concentrates points near the critical layer at the expense of nodes near the wall, counters somewhat the effect of the algebraic mapping. The higher grid resolution required in the initial stages of the simulation due to high gradients in the density and temperature perturbation profiles in the critical layer region also increases the total CPU time. And last, but not least, compressibility effects weakens the instability. Second mode waves have a high spatial and temporal frequency. With the chosen parameters, the wave linearly grows by a factor of 1.06 every period. In the absence of non-linear effects, over 150 periods are required to achieve an amplification of e^9, compared with less than 10 periods at low subsonic speeds. With an explicit code, simulation of 25 periods on a $8 \times 2 \times 65$ grid requires approximately 10 CPU hours of Cray 2 at sustained speeds of 80 Mflops. At this stage, the growth of a single 2-D 2nd mode wave is still quasi-linear, and has only amplified by a factor 4.

A. *Modal Analysis*

One of the many issues encountered in the treatment of compressible flows is the generalization of modal energy, and intermodal energy transfer. These concepts are the backbone of incompressible transition theories [8]. Modal energy leads to the concept of energy cascade in turbulence [23], and permits the energy exchange processes between different modes to be computed. The standard definition of modal energy in incompressible flows is a consequence of the quadratic form of the kinetic energy. Let

$$E = \int \vec{v}(x,y)^2 \, dx \, dy = cst \int |\hat{\vec{v}}(k,y)|^2 \, dk \, dy \tag{27}$$

be the total kinetic energy in the system, where the second equality is a consequence of Parseval's identity. $\vec{v}(x,y)$ and $\hat{\vec{v}}(k,y)$ are Fourier Transforms of one another. The constant cst is inconsequential. The above definition of kinetic energy suggests that

$$E_k = cst \int |\hat{\vec{v}}_k(k,y)|^2 \, dy \tag{28}$$

be interpreted as the integrated kinetic energy in mode k. Such a definition is no longer valid for compressible flows. The kinetic energy is now defined by the cubic nonlinearity

$$E = \tfrac{1}{2} \int \rho(x,y) \vec{v}(x,y)^2 \, dx \, dy \tag{29}$$

which becomes in transformed space

$$E = cst \int \hat{\rho}(k,y) \hat{\vec{v}}(l,y) \vec{v}(-k-l,y) \, dk \, dl \, dy \tag{30}$$

which does not have a straightforward representation of the form

$$E = \int E(k) \, dk \tag{31}$$

One remedy, although not altogether justifiable, is to rewrite the kinetic energy as the product of velocity $\vec{v}$ and momentum $\vec{m}$. For example, the kinetic energy of a photon must be defined this way because it is massless. If such a definition is accepted, the kinetic energy in mode k (intuitively) becomes

$$E_k = cst \int (\hat{\vec{m}}(k,y) \hat{\vec{v}}(-k,y) + c.c) \, dy \tag{32}$$

where the complex conjugate $(c.c)$ is to insure that E_k is real. It is then possible to determine contributions of any mode to any other mode. An equation describing the time evolution of E_k can be derived, and intermodal transfer of kinetic energy determined. Of course it is by no means obvious that this is the physically appropriate definition for E, although it does reduce to the accepted form of the modal energy in the limit of zero Mach number. Another issue is: what fraction of internal energy is contained in each mode? The internal energy density is a quadratic function in ρ and T; therefore, a definition similar

to that of E_k is possible. However, why should the internal energy be defined in terms of an energy density, while the kinetic energy is not? Ideally, the modal energy of different energy types should have consistent definitions.

Experimentalists measure energy growth [10] (in the streamwise direction) in several ways, mostly with hot wire anemometry. The wire can be translated downstream at a constant height (y=const) above the plate. Alternatively, at each streamwise station, the y location can correspond to maximum growth of a specified variable. The growth rate can also be integrated in the y direction. Numerically, any one of these options is possible. We choose to calculate the instantaneous growth rate of the fundamental mode at each y location. Different variables have different growth rates and instantaneous growth rate of any variable can be measured. In this paper, only the growth of the streamwise velocity is considered because the presence of a critical layer might lead to interesting results.

At any instant in time, say t^*, $\hat{u}$(k,y,t) has the representation

$$\hat{u}(k,y,t^*+t) = \tilde{u}(k,y)e^{-\iota\sigma(y,t)t} \tag{33}$$

so that the growth rate is simply

$$\sigma(y,0) = \iota \left.\frac{\dot{u}}{u}\right|_{t=0} \tag{34}$$

By comparing Eq. (34) with the growth rate computed from

$$\sigma(y,t^*) = \frac{\iota}{t}\log\frac{u(k,y,t^*+t)}{u(k,y,t^*)}, \tag{35}$$

the degree of linearity can be measured as a function of t. If the growth of mode k is purely linear, both formulas will agree for all values of t.

VI. Results

In this paper, all results pertain to a fixed set of physical parameters. The free-stream Mach number is 4.5, $T_\infty = 110°R$, $Re = 8000$ (based on δ^*), $\alpha = 2.25$ and $\beta = 0.0$. The choice of wavenumbers is motivated by the maximum temporal growth rate of 2-D second mode perturbation waves. The streamwise wavenumber produces the largest linear growth rate at the specified Reynolds number.

The linear eigenfunctions were obtained from SPECLS [14] which solves the linearized Navier-Stokes equations with a spectral algorithm. Spectral initial conditions are necessary to prevent slight numerical oscillations in the mean flow and in the computed linear eigenfunction. Otherwise the non-linear calculation might be contaminated. Figures 1a-f compare the amplitude and phase plots of u, v, and T eigenfunctions of an unstable 2-D first mode wave ($\alpha = 0.6, \beta = 0, Re = 10000, T_\infty = 110°R$) with the unstable second mode

defined above. The major differences between first and second mode disturbances are: 1) the first mode is viscous below a Mach number of about 3-4, and is nearly inviscid at higher Mach numbers, the second mode is always inviscid in nature; 2) the second mode phase velocity is close to unity; and 3) 3-D first modes are most unstable at angles between 55° and 65° with respect to the mean flow, while 2-D second mode waves are most unstable. Another feature worth noting for the particular choice of parameters, is the large vertical velocity component in the 2nd mode eigenfunction compared to that in the 1st mode wave. These differences might be explained by the factor 4 ratio of second to first mode streamwise wave numbers. As expected from Mack's results, the second mode waves decay much faster than the 1st mode. The first mode waves decay on a viscous scale, while the 2nd mode decays on the inviscid scale. The 180° phase jumps in streamwise velocity occur in opposite directions (i.e. increasing towards the free-stream for the 2^{nd} mode, and decreasing for the 1^{st} mode). The significance of this, if any, is not known.

The eigenfunctions calculated by the linear code are assumed to satisfy

$$u_{pert}(x, y, z) = u'(y)e^{i(\alpha x - \omega t)} \tag{36}$$

so that the real part of ω, (ω_r) is the wave frequency and its imaginary part (ω_i) the growth rate. The wave is unstable if ω_i is positive. The linear eigenvalue for the second mode perturbation used in the non-linear simulation is

$$\begin{aligned} \omega_r &= 2.046738 \\ \omega_i &= 2.149042\,10^{-2} \end{aligned}$$

Based on the 2-D wave frequency, the temporal period is 3.07 in non-dimensional time units. From here on, time is always expressed in units in 2-D wave periods. Based on the above parameters, the streamwise phase velocity is $c = 0.91$, which corresponds to a critical layer located at $y = 1.10$. The mean flow profile also has a generalized inflection point [‡] at $y = 1.06$. The mean temperature across the boundary layer varies by more than a factor of 4. This is in sharp contrast with the slowly varying mean temperature profiles at low subsonic Mach numbers.

To test the code against linear theory, an initial eigenfunction with a 0.1% amplitude is superimposed on the mean flow and its evolution followed up to $t = 3$. The growth rate ω_i and frequency (ω_r) are shown in figures 2a-b. The growth rate varies less than 0.4% over the interval $0 < y < 2$. The frequency has a 0.1% variation in the same range of y. Integrated value of growth, when compared against prediction of linear theory, shows 4 decimal place agreement. In all the runs discussed, accuracy of the solution is measured from plots of the the L_2 norm of the Chebyshev series coefficients (integrated in the streamwise direction) versus the wavenumber. Grid resolution is chosen to insure that these spectra decrease by at least 8 orders of magnitude.

Next, results from a run with a $\epsilon_{2D} = 0.02$ amplitude for streamwise perturbation

[‡]The generalized inflection point is the vertical coordinate y at which $d/dy(\rho_m(y)d/dy(U_m(y))) = 0$.

velocity, which is fairly large, are presented. The corresponding initial density fluctuation level is 9.2%

One non-linear simulation of 25 periods in time was performed and the results are presented below. Initial streamwise velocity and density amplitude levels are 2% and 9.2%. The remaining figures show the state of selected quantities at t=0,5,10,15 and 20 (unit of time is one period). Figures 3a-b show the growth rate and frequency of the fundamental streamwise velocity, u_{10}, labeled (1,0) for simplicity and to emphasize the two dimensionality of the problem. (In general, (k,0) refers to the kth mode, and (0,0) to the instantaneous mean flow.) The growth rate and the frequency are obtained from the coefficient of $e^{\iota\alpha x}$ of the Fourier expansion of u calculated at two successive time levels. The major feature of interest is the sharp decrease in the local growth rate near the critical layer ($y = 1.1$). After a slight initial increase, the growth rate starts decreasing. If the growth rate reaches zero, the (1,0) mode will have reached a saturated state. The frequency, and therefore the phase velocity is decreasing slightly towards zero, albeit at a slower rate than the growth rate (fig. 3b). The growth rate and frequency show a marked change near the wall at period 0. There are several possible reasons for this, but the phenomena has not been looked into in detail. Typically, numerically generated growth rates are obtained from the integrated energy, which wipes out any oscillations due to inconsistent or inaccurate initial conditions. The mean flow and the initial profiles were obtained spectrally, with two different codes and grids, and spectral interpolation was performed to transfer information from one grid to another. Because the mean flow was computed on a smaller grid than were the fundamental profiles, the interpolation generated slight oscillations in the second derivative of the mean flow. This in turn affects the local growth profiles. It is obvious however from the figure that the initial slight inconsistencies are washed away at later times. Note the sharp peak near the critical layer. To understand better the origin of this critical layer structure, Fourier transform the streamwse momentum equation in the x direction, and only consider the terms that contribute to the fundamental mode. Neglecting the viscous terms, this leads to the equation

$$\rho_0 u_{1t} + \iota\alpha(\rho_0 u_0 u_1 + p_1) + \rho_0(v_1 u_{0y} + v_0 u_{1y})\iota\alpha\rho_{-1}u_1^2 + \rho_{-1}v_1 u_{1y} + \rho_1(v_1 u_{-1y} + v_{-1}u_{1y}). \quad (37)$$

if u_1 is assumed to vary as $e^{-\iota\omega t}$ (where ω is a function of y and t), the instantaneous growth rate and frequency are obtained through after dividing this equation by $\rho_0 u_1$:

$$-\iota\omega = \text{linear terms} + \text{cubic terms} \quad (38)$$

where

$$\text{linear terms} = \iota\alpha(u_0 + \frac{p_1}{u_1}) + \frac{v_1 u_{0y} + v_0 u_{1y}}{u_1} \quad (39)$$

and

$$\text{cubic terms} = \iota\alpha\frac{\rho_{-1}u_1}{\rho_0} + \frac{\rho_{-1}v_1 u_{1y} + \rho_1(v_1 u_{-1y} + v_{-1}u_{1y})}{\rho_0 u_1} \quad (40)$$

The growth rate is the real part of Eq. (38). The linear terms contribute a zeroth order growth rate, while the growth rate due to the cubic nonlinearities is quadratic in the

amplitude of the fundamental mode. In figures 4a-b, the growth rate ω_r is plotted as a function of the normal coordinate y. Figure 4a plots the combination of linear terms, excluding the viscous interaction, which explains the sharp increase in growth near the origin and the structure at the critical layer, which are removed by the viscous effects. If the viscous effects were included, and the wave amplitude sufficiently small, figs. 4a and 2a would be identical. Cubic nonlinearities are plotted in figure 4b. One notes the absence of growth rate everywhere, except in the critical layer and in a thin layer near the wall. The nonlinearities near the wall can be explained by consideration of the viscous terms. The viscosity is a function of temperature and becomes, after taylor expansion,

$$\mu(T) \approx \mu_0 + \mu_{0T} T_1 + \tfrac{1}{2} T_{-1} T_1 \mu_{0TT} + \tfrac{1}{2} T_{-1} T_1^2 \mu_{0TTT}. \tag{41}$$

Derivatives of the mean viscosity μ_0 with respect to the mean temperature are denoted by the subscripts T. Since the viscous stress terms are quadratic in the viscosity and the primitive variables, only the mean and fundamental components of viscosity need be retained. The terms that contribute to the linear equations (in the fundamental amplitude) are

$$\mu_0 + \mu_{0T} T_1 \tag{42}$$

while

$$\tfrac{1}{2} T_{-1} T_1 \mu_{0TT} + \tfrac{1}{2} T_{-1} T_1^2 \mu_{0TTT} \tag{43}$$

contributes to the cubic nonlinearities. The cubic nonlinearities drop out if μ is independent of temperature. More detailed mapping of these various terms is under progress. Figures 5-7 show the fundamental, first harmonic, and distorted mean profiles. A comparison of fig. 5a and fig. 5c shows that u_1 and ρ_1 grow at different rates. Initially, u_1 has a normalized maximum of 0.01, and ρ has its maximum at 0.046, i.e. a ρ_1 to u_1 ratio of 4.6. At $t = 20$, this ratio is 2.62, indicating that the peak u_1 grows faster than the peak ρ_1. Of course these growth rates may be governed by different processes. Near the wall, viscous effects dominate, while ρ has its maximum at the critical layer, where the cubic interactions dominate. The mean vertical flow is plotted in fig. 6 and has two strong peaks. Near the wall, the peak is broad, compared to the narrow peak near the critical layer. These structures are best explained by a perturbation methods approach, which is currently under investigation. Figures 7a-c show the first harmonic components of u, v, ρ. The maximum amplitude of these waves is approximately an order of magnitude smaller than that of the fundamental. This suggests that a weakly non-linear asymptotic theory is sufficient to predict the evolution of a single two-dimensional mode, perhaps including the structure of its saturated state. To support this hypothesis, a second calculation was performed with the same initial conditions. However, all streamwise modes above the fundamental were set to zero after each iteration [§]. Growth rate curves at $t = 10$ are virtually identical to that shown in fig. 3. This indicates that the higher streamwise modes only play a secondary role in the evolution towards a saturated state. As shown above, the leading role is that due to the cubic nonlinearities in the momentum equation A perturbation analysis should allow a large number of parametric studies relatively cheaply. Contributions to the growth

[§]More precisely they were set to zero at each stage of the 3rd order Runga-Kutta algorithm

rate from various sources will be determined, and the simulation carried out further than otherwise possible.

Finally, it is interesting to understand the mechanisms that pertain to vorticity production. The compressible analogue to the incompressible vorticity equation is

$$\frac{\partial \vec{\omega}}{\partial t} + \vec{v} \cdot \nabla \vec{\omega} = \vec{\omega} \cdot \nabla \vec{v} - \vec{\omega} \nabla \cdot \vec{v} - \nabla \rho^{-1} \times \nabla p + 2\mu \nabla \times \left[\rho^{-1} \nabla \cdot (\vec{\vec{\tau}} - \tfrac{1}{3} \nabla \cdot \vec{v} \vec{\vec{I}}) \right] \qquad (44)$$

where $\vec{\omega} = \nabla \times \vec{v}$. Terms not present in the limit of incompressibility are the dilatation term $\vec{\omega} \nabla \cdot \vec{v}$ and the baroclinic torque $\nabla \rho^{-1} \times \nabla p$. The vorticity production due to dilatation and baroclinic torque (average over streamwise direction) are shown in figs 8a-b. Figure 8c shows the combined effects of dilation, convection and baroclinic torque on the production of vorticity. In all 3 plots, the production of vorticity is localized in the near wall region, and at the critical layer. The rms perturbation vorticity is shown in fig. 9 after 20 periods (after subtraction of the mean flow vorticity).

VII. Conclusions

A three-dimensional, fully spectral code developed for the direct simulation of the wall-bounded compressible flows has been applied to the nonlinear evolution of a single unstable second mode wave. After an slight initial growth, the growth rate of this fundamental wave decreases in time. This suggest that the second mode is evolving towards a saturated state. Perturbation methods are sometimes well-suited for the study of such states. To ascertain whether such an approach is called for, all streamwise modes above the fundamental were continuously set to zero at every time step. This led to a time evolution of the fundamental waves almost identical with the case where all modes were allowed to interact with each other. This agreement was also found for the structure of the time-dependent instantaneous growth rate of u, even in the critical layer region. The conclusion is that the cubic interaction terms that only involve the fundamental waves are probably responsible for the nonlinearities in the critical layer, and that the density fluctuations play a fundamental role.

A final note. The initial perturbation wave was chosen to maximize its instability. Nayfeh [20] found that stable 2-D second mode waves were susceptible to strong secondary instabilities. It is therefore still not clear which are the actual waves that will be most responsible for the final transition towards turbulence. These issues will be addressed in the future.

VIII. Acknowledgements

One of the authors is thankful for fruitful discussions with Drs. L. Ng, B. Singer, C.L. Streett, and T.A. Zang. This problem was suggested by M. Morkovin.

References

[1] Beckwith, I.E.; Chen, F.J; and Malik, M.R., Jr.: Design and Fabrication Requirements for Low-Noise Supersonic/Hypersonic Wind Tunnels. AIAA Paper N. 88-0143, presented at the AIAA 26th Aerospace Sciences Meeting, Reno, Nevada, January 11-14, 1988.

[2] Canuto, C.; Hussaini, M. Y.; Quarteroni, A.; and Zang, T. A.: *Spectral Methods in Fluid Dynamics*, Springer-Verlag, Berlin, 1987.

[3] Demetriades, A.: Laminar Boundary Layer Stability Measurements at Mach 7 including Wall Temperature Effects. AFOSR 77-1311, 63 pp., 1977.

[4] El-Hady, N.M.: Secondary Three-Dimensional Instability in Compressible Boundary Layers. Proceedings of the Transonic Symposium, Theory, Application and Experiment, 1988, to appear.

[5] Erlebacher, G: Transition Phenomena over a Flat Plate for Compressible Flows. *Tenth International Conference on Numerical Methods in Fluid Dynamics*, Springer Verlag, F.G. Zhuang and Y.L. Zhu (Eds.), Berlin, 1986.

[6] Erlebacher, G.; and Hussaini, M. Y.: Incipient Transition Phenomena in Compressible Flows over a Flat Plate, ICASE Report 86-39, 1986.

[7] Erlebacher, G. and Hussaini, M.Y.: Stability and Transition in Supersonic Boundary Layers. AIAA paper AIAA-87-1416, presented at the 19th Fluid Dynamics, Plasma Dynamics and Lasers Conference in Hawaii, 1987.

[8] Herbert, T.: Floquet analysis of secondary instability in shear flows, *Stability of Time Dependent and Spatially Varying Flows*, D. L. Dwoyer and M. Y. Hussaini (Eds.), pp. 43-57, Springer Verlag, New York, 1987.

[9] Hussaini, M. Y.: Stability, Transition and Turbulence. *Supercomputing in Aerospace*, NASA Conference Publ. 2454, pp. 211-220, 1987.

[10] Kendall, J. M.: Wind Tunnel Experiments Relating to Supersonic and Hypersonic Boundary Layer Transition. *AIAA Journal*, Vol. 13, pp. 240-299, 1975.

[11] Kovasznay, L.S., Komoda, H. and Vasudeva, B.R., *Proc. of the 1962 Heat Transfer and Fluid Mech.* Inst., pp. 1-26, Stanford University Press, 1962.

[12] Laufer, J. and Vrebalovich, T.: Stability and Transition of a Supersonic Laminar Boundary Layer on an Insulated Flat Plate. *J. Fluid Mech.*, Vol. 9 pp. 257-299, 1960.

[13] Lees, L. and Lin, C. C.: Investigation of the Stability of the Laminar Boundary Layer in a Compressible Fluid. NACA Tech. Note No. 1115, 1946.

[14] Macaraeg, M., Streett, C.L. , and Hussaini, M.Y.: A Spectral Multi-Domain Technique Applied to High-Speed Chemically Reacting Flows. Proceedings of the 2nd International Symposium on Domain Decomposition Methods, Los Angeles, CA, Jan. 14-16,1988.

[15] Mack, L. M.: Computation of the Stability of the Laminar Boundary Layer. *Methods in Computational Physics*, Eds. B. Alder, S. Fernbach and M. Rotenberg, Vol. 4, pp. 247-299, Academic, N.Y., 1965.

[16] Mack, L. M.: Boundary-Layer Linear Stability Theory. AGARD, Report 709, 1984.

[17] Mack, L. M.: Review of Linear Compressible Stability Theory. *Stability for Time Dependent and Spatially Varying Flows*, D.L. Dwoyer and M.Y. Hussaini (Eds.), Springer Verlag, New York, pp. 164-187, 1985.

[18] Malik, M.R.: Finite-Difference Solution of the Compressible Stability Eigenvalue Problem. NASA Contractor Report 3584, 1982.

[19] Morkovin, M. V.: Fluctuations and Hot-Wire Anemometry in Compressible Flows. AGARDograph 24, 102 pp., 1957.

[20] Nayfeh, A.H.: Stability of Compressible Boundary Layers. Proceedings of the Transonic Symposium, Theory, Application and Experiment, NASA CP 3020, Vol. I, 1989.

[21] Quateroni, A.: private communication.

[22] Stetson, K. F.; Thompson, E. R.; and Donaldson, J. C.: Laminar Boundary Layer Stability Experiments. AIAA paper AIAA-83-1761, 1983.

[23] Tennekes, H. and Lumley, J.L: *A First Course in Turbulence*. Eighth printing, MIT Press, 1982.

[24] Wray, A. and Hussaini, M.Y.: Numerical experiments in Boundary-layer Stability. *Proc. R. Soc. Lond.*, Vol. 392, pp. 373–389, 1984.

[25] Zang, T.A. and Hussaini, M.Y.: Numerical Experiments on the Stability of Controlled Shear Flows. AIAA paper 85-1698, 1985.

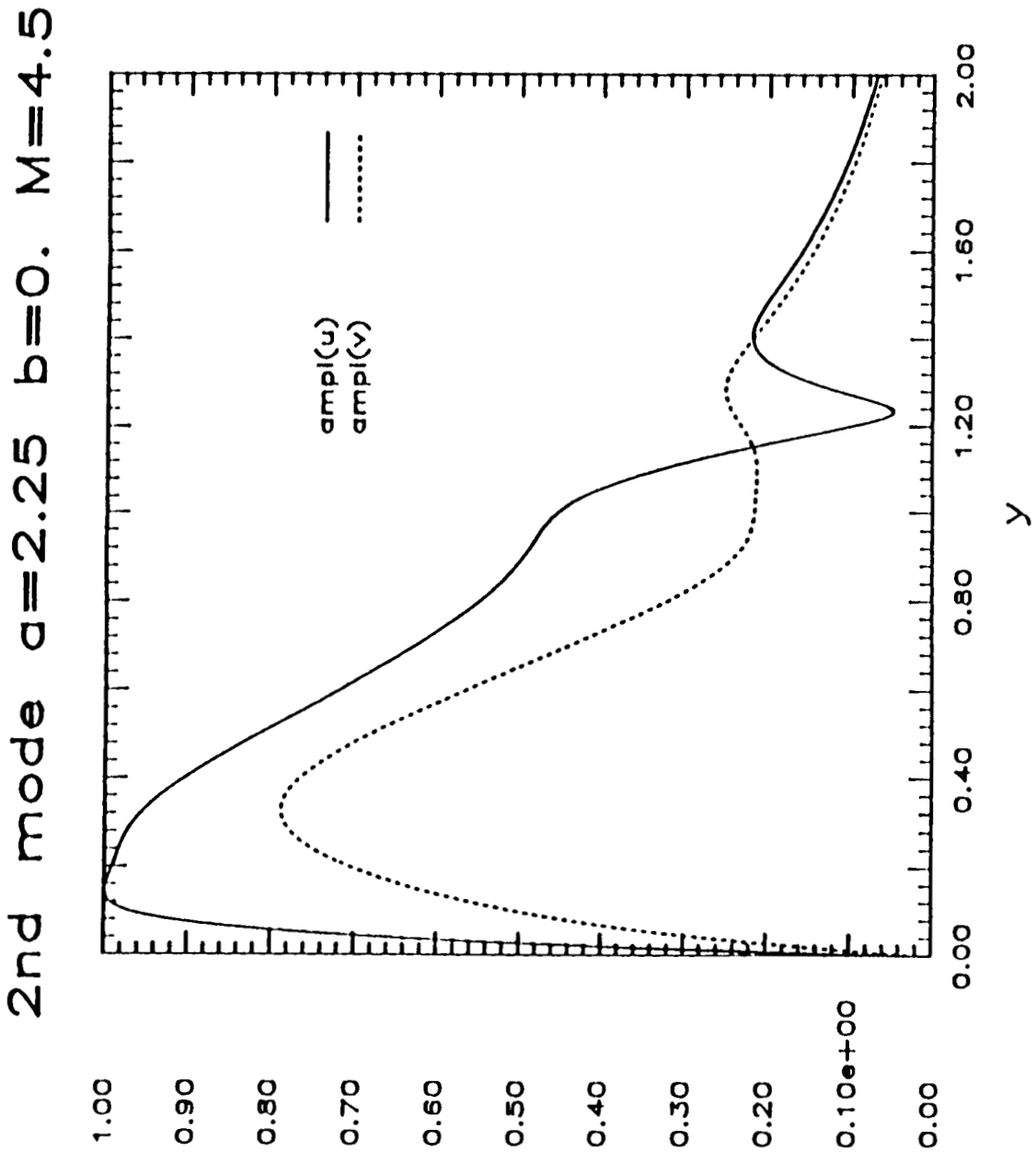
2nd mode a=2.25 b=0. M=4.5
ampl(u)
ampl(v)
1.00
0.90
0.80
0.70
0.60
0.50
0.40
0.30
0.20
0.10e+00
0.00
0.00
0.40
0.80
1.20
1.60
2.00
y

Figure 1a

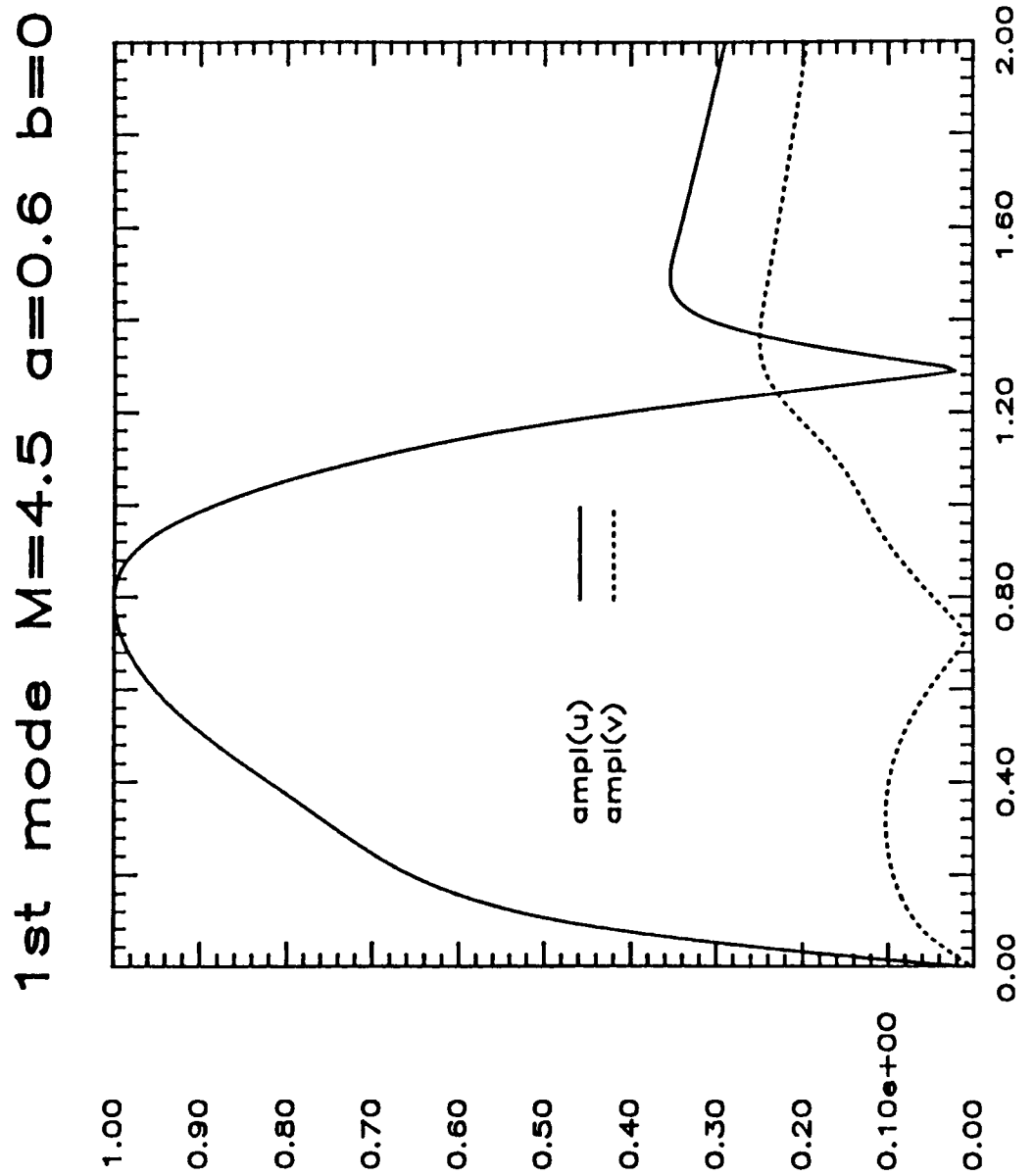
1st mode M=4.5 a=0.6 b=0
ampl(u)
ampl(v)
y
0.00
0.40
0.80
1.20
1.60
2.00
0.00
0.10e+00
0.20
0.30
0.40
0.50
0.60
0.70
0.80
0.90
1.00

Figure 1b

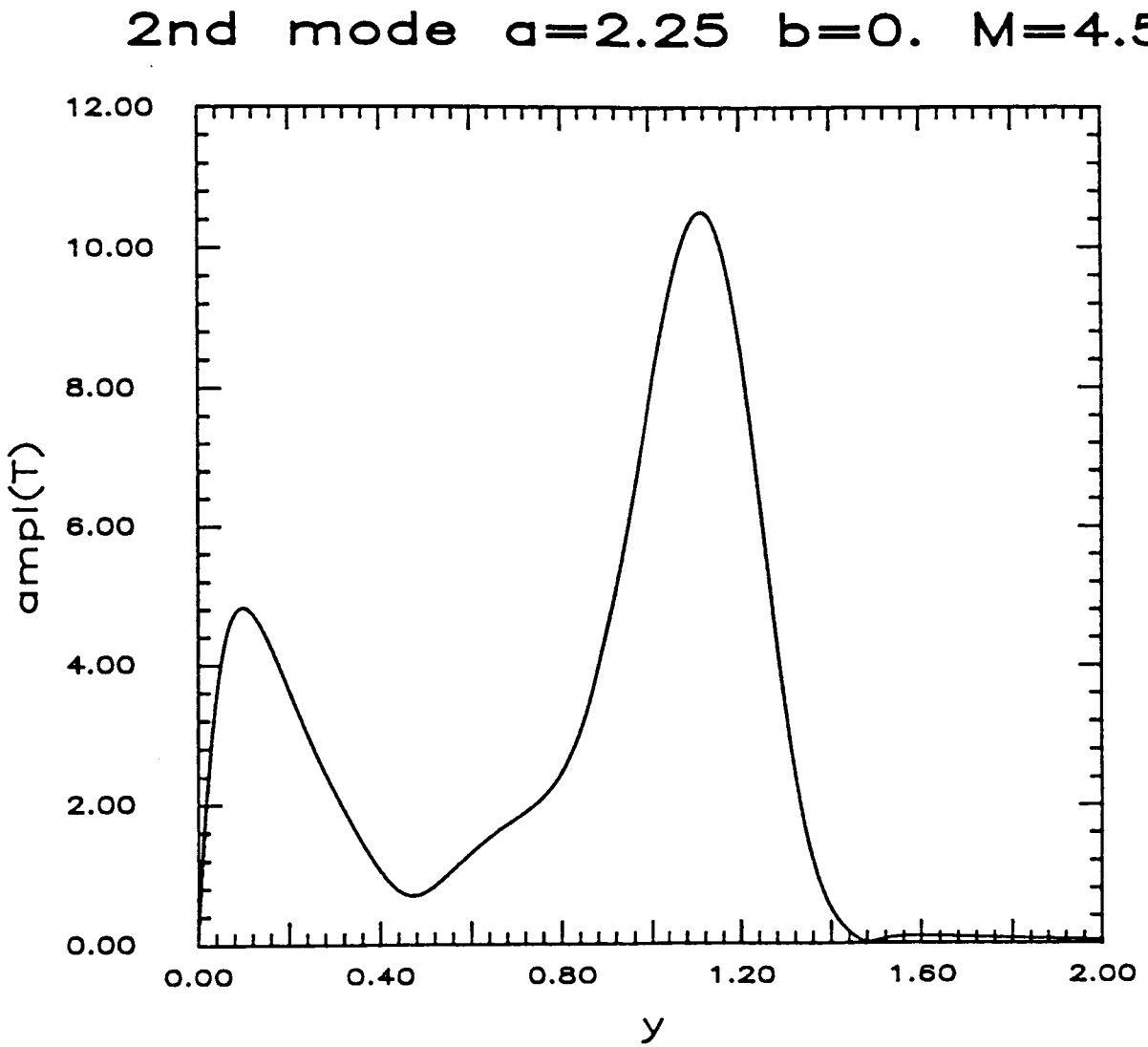
2nd mode a=2.25 b=0. M=4.5
12.00
10.00
8.00
6.00
4.00
2.00
0.00
ampl(T)
0.00
0.40
0.80
1.20
1.60
2.00
y

Figure 1c

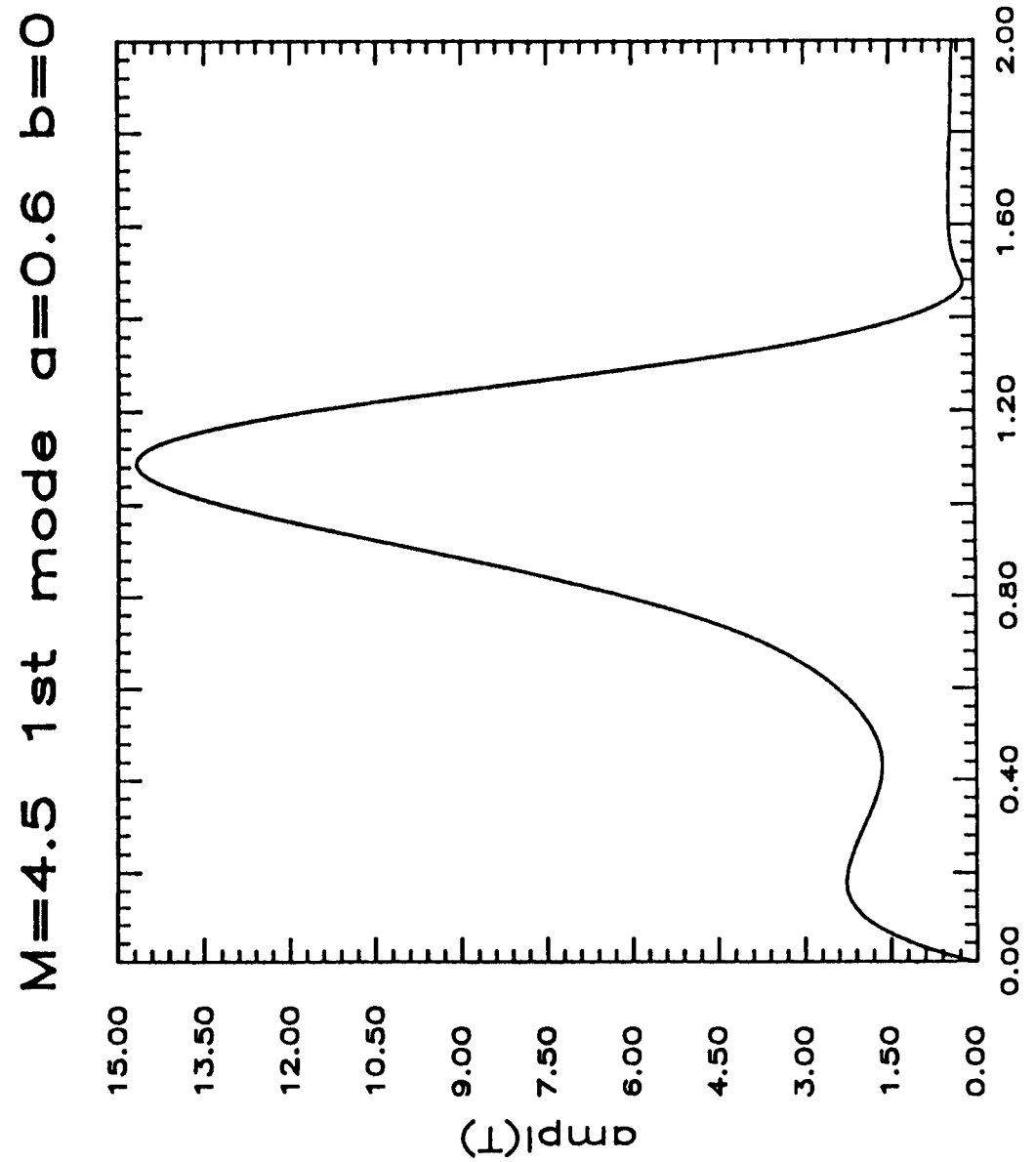
M=4.5 1st mode a=0.6 b=0
ampl(T)
15.00
13.50
12.00
10.50
9.00
7.50
6.00
4.50
3.00
1.50
0.00
0.00
0.40
0.80
1.20
1.60
2.00
y

Figure 1d

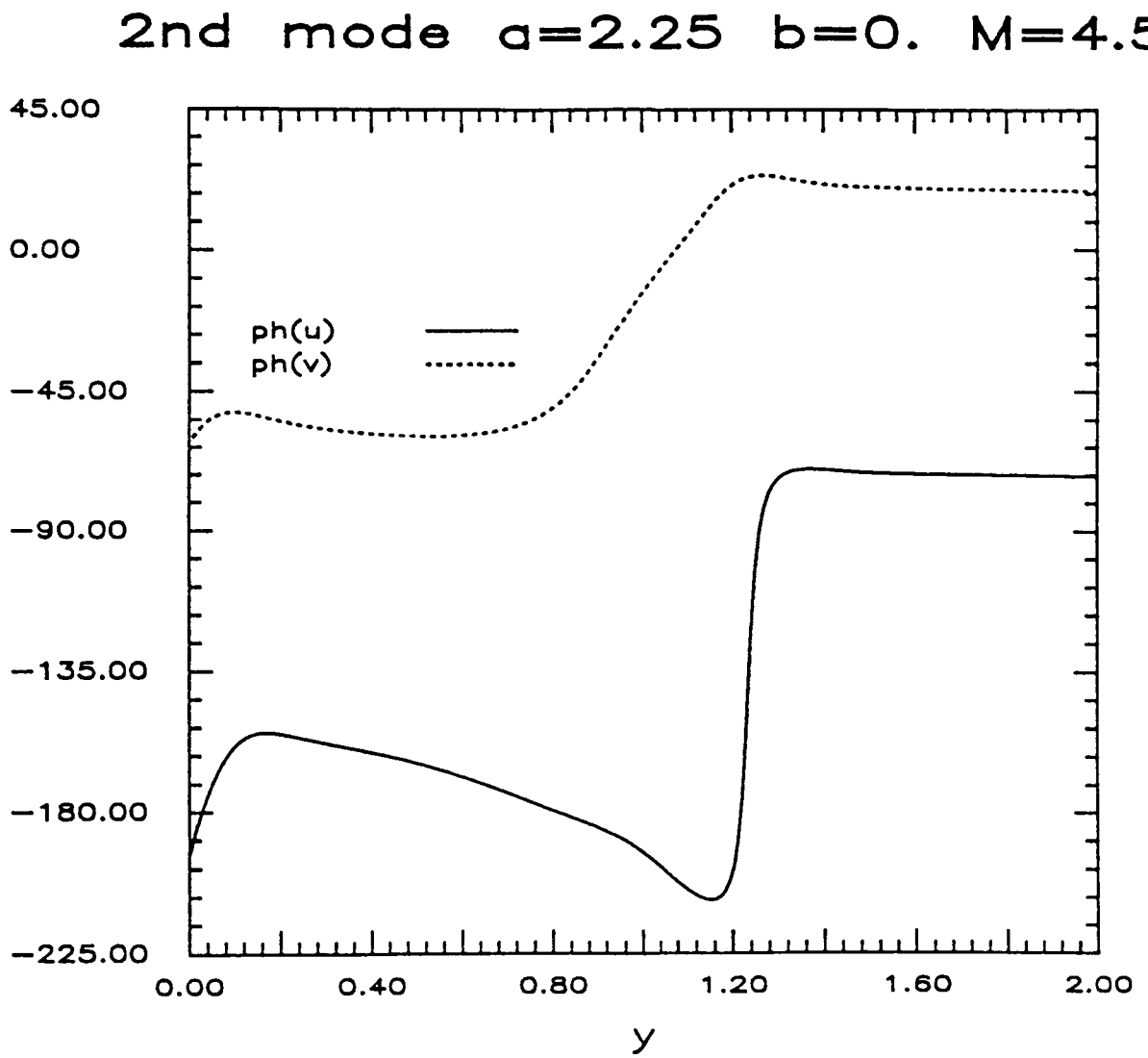
2nd mode a=2.25 b=0. M=4.5
45.00
0.00
−45.00
−90.00
−135.00
−180.00
−225.00
ph(u)
ph(v)
0.00
0.40
0.80
1.20
1.60
2.00
y

Figure 1e

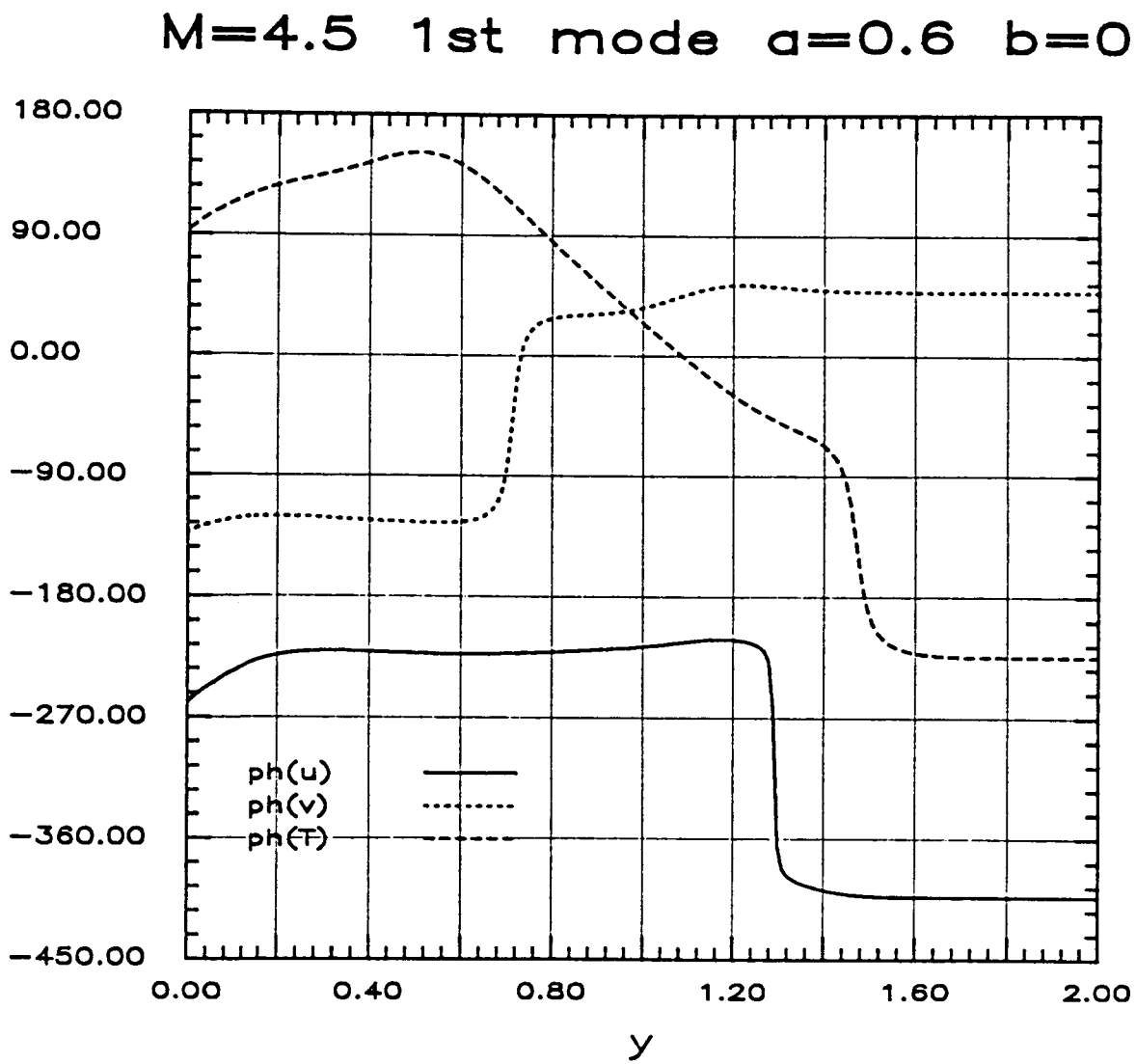
M=4.5 1st mode a=0.6 b=0
180.00
90.00
0.00
−90.00
−180.00
−270.00
−360.00
−450.00
0.00
0.40
0.80
1.20
1.60
2.00
y
ph(u)
ph(v)
ph(T)

Figure 1f

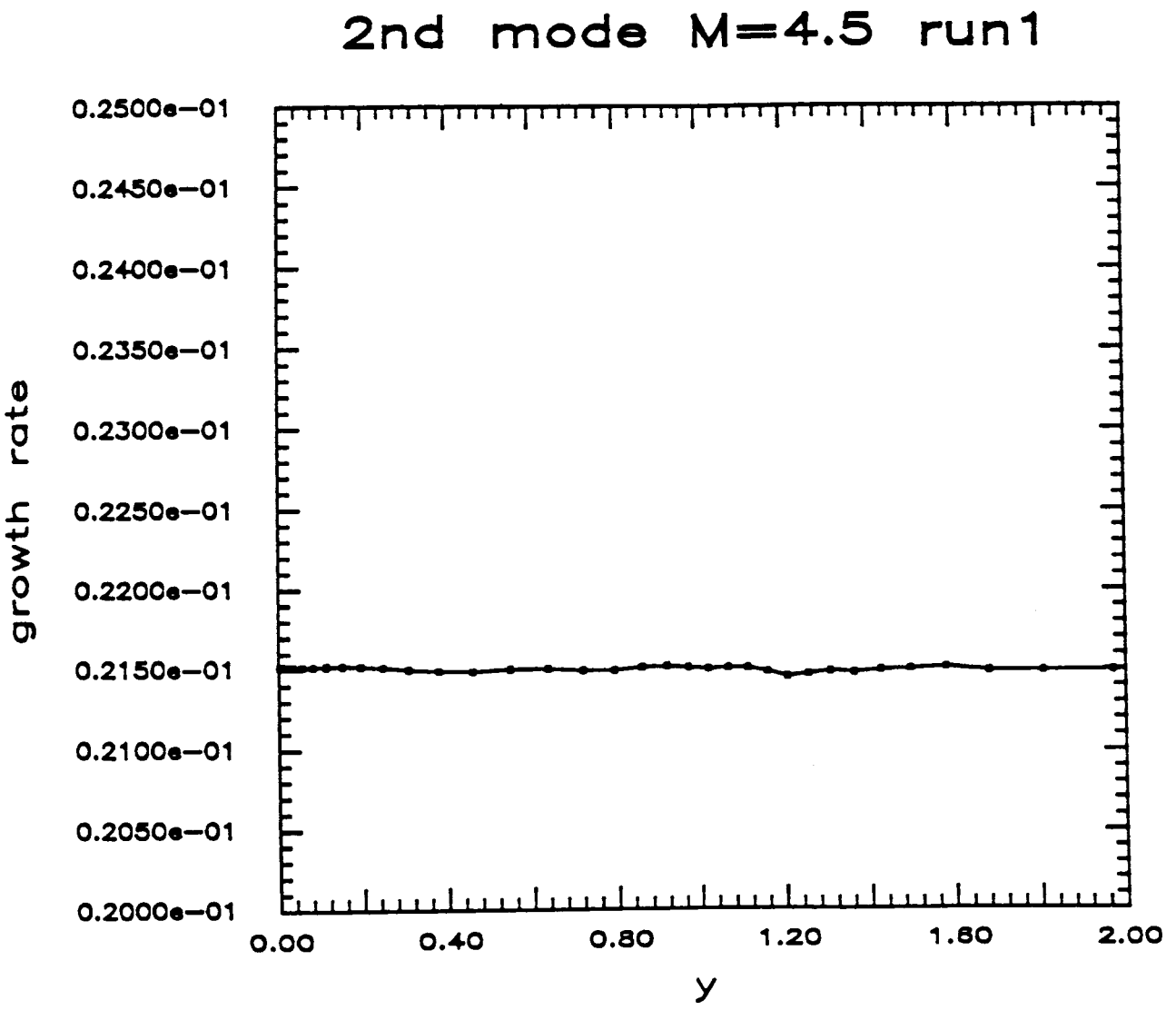
2nd mode M=4.5 run1
growth rate
0.2500e-01
0.2450e-01
0.2400e-01
0.2350e-01
0.2300e-01
0.2250e-01
0.2200e-01
0.2150e-01
0.2100e-01
0.2050e-01
0.2000e-01
0.00
0.40
0.80
1.20
1.60
2.00
y

Figure 2a

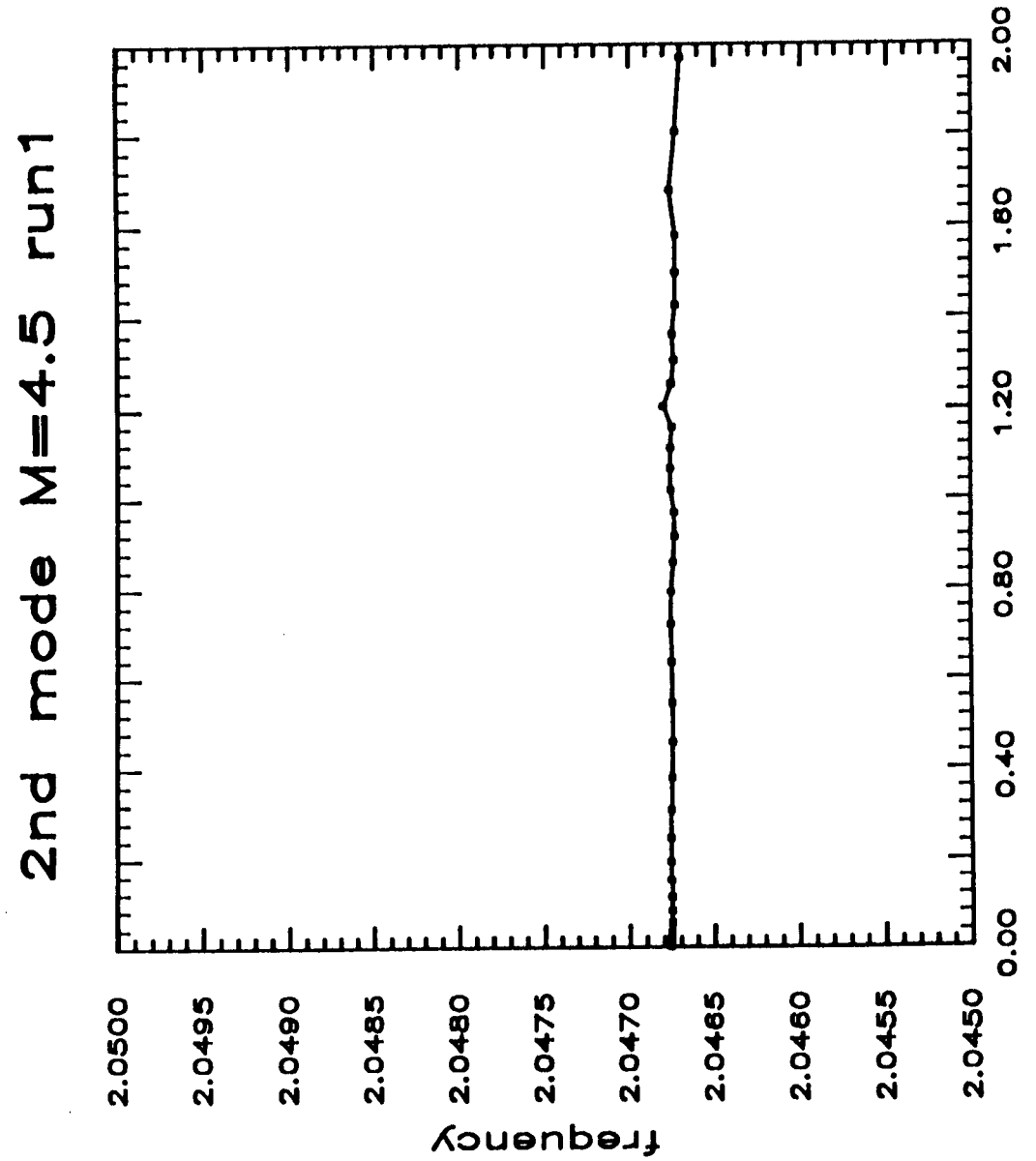
2nd mode M=4.5 run1
frequency
2.0500
2.0495
2.0490
2.0485
2.0480
2.0475
2.0470
2.0465
2.0460
2.0455
2.0450
0.00
0.40
0.80
1.20
1.80
2.00
y

Figure 2b

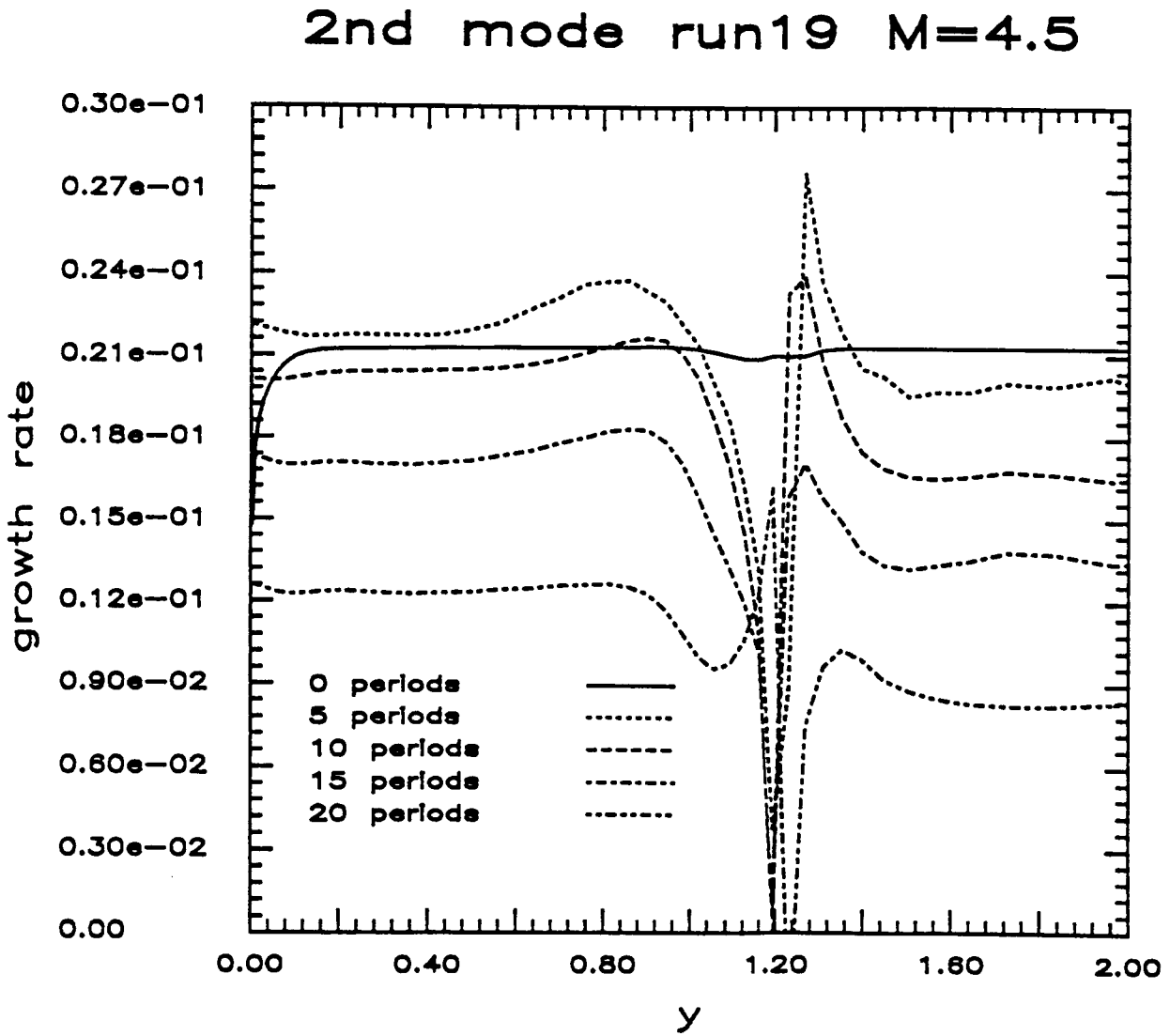
2nd mode run19 M=4.5
0.30e-01
0.27e-01
0.24e-01
0.21e-01
0.18e-01
0.15e-01
0.12e-01
0.90e-02
0.60e-02
0.30e-02
0.00
growth rate
0 periods
5 periods
10 periods
15 periods
20 periods
0.00
0.40
0.80
1.20
1.60
2.00
y

Figure 3a

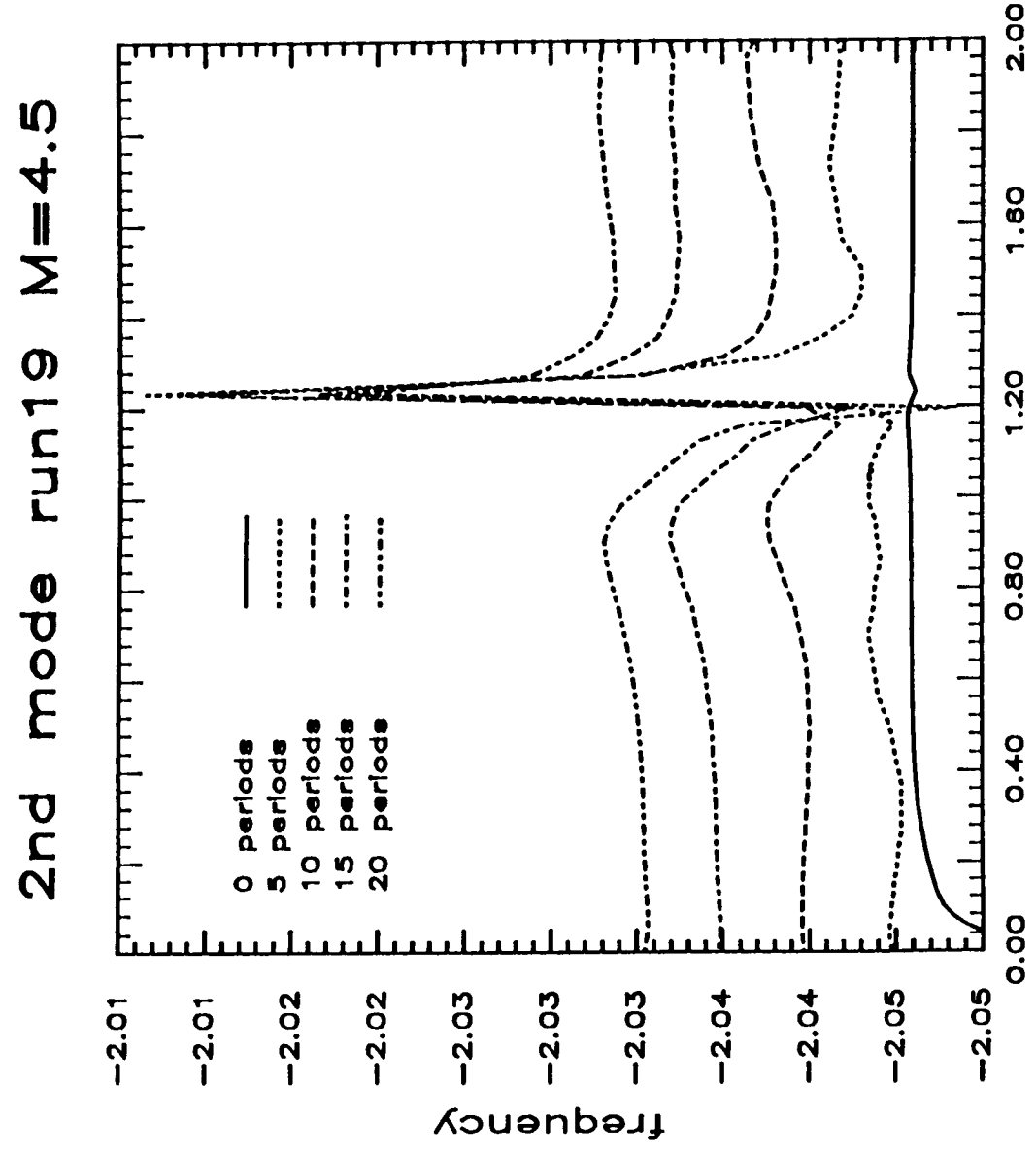
2nd mode run19 M=4.5
0 periods
5 periods
10 periods
15 periods
20 periods
frequency
y
-2.01
-2.01
-2.02
-2.02
-2.03
-2.03
-2.04
-2.04
-2.05
-2.05
0.00
0.40
0.80
1.20
1.60
2.00

Figure 3b

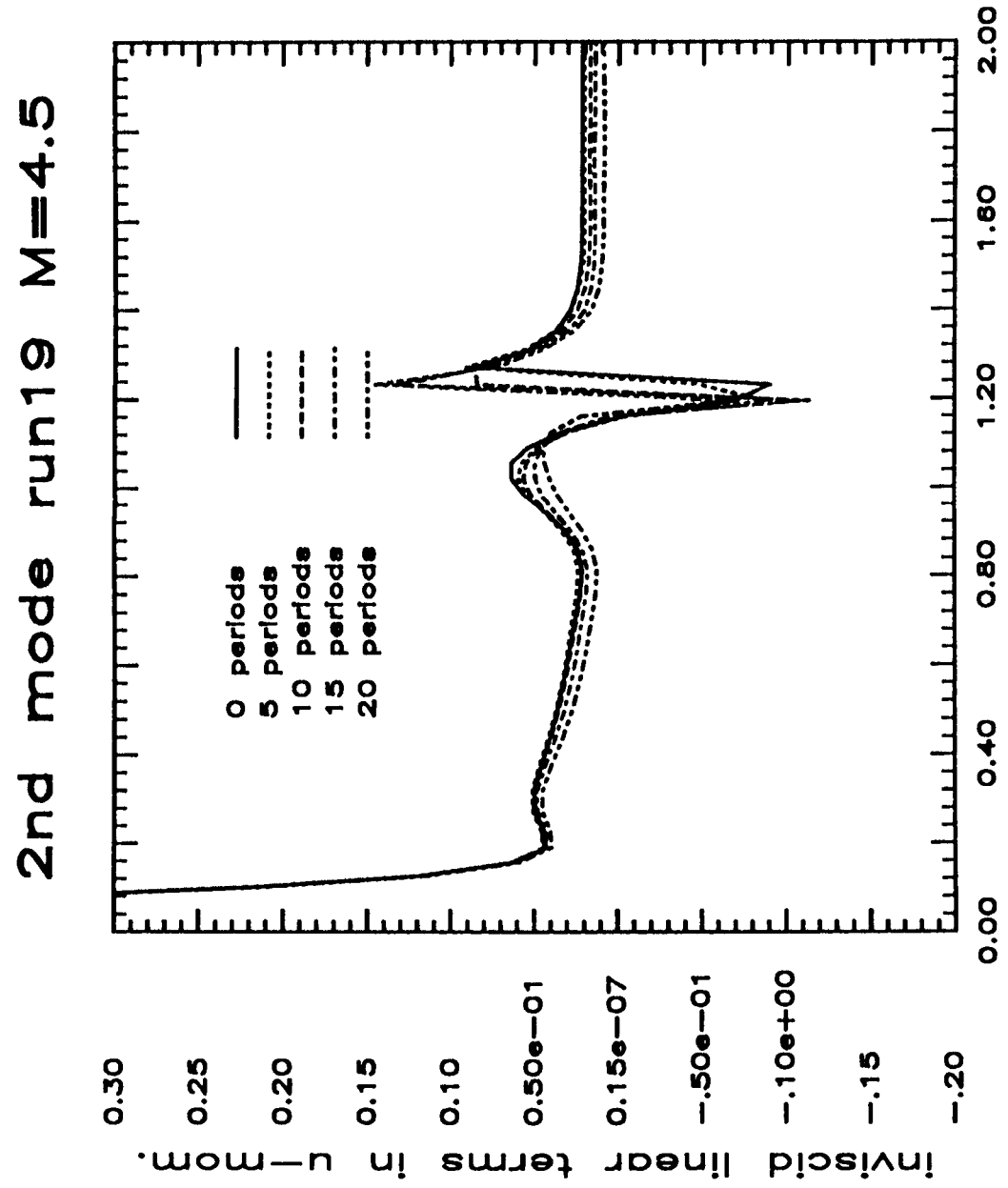
2nd mode run19 M=4.5
0 periods
5 periods
10 periods
15 periods
20 periods
inviscid linear terms in u-mom.
0.30
0.25
0.20
0.15
0.10
0.50e-01
0.15e-07
-.50e-01
-.10e+00
-.15
-.20
0.00
0.40
0.80
1.20
1.80
2.00
y

Figure 4a

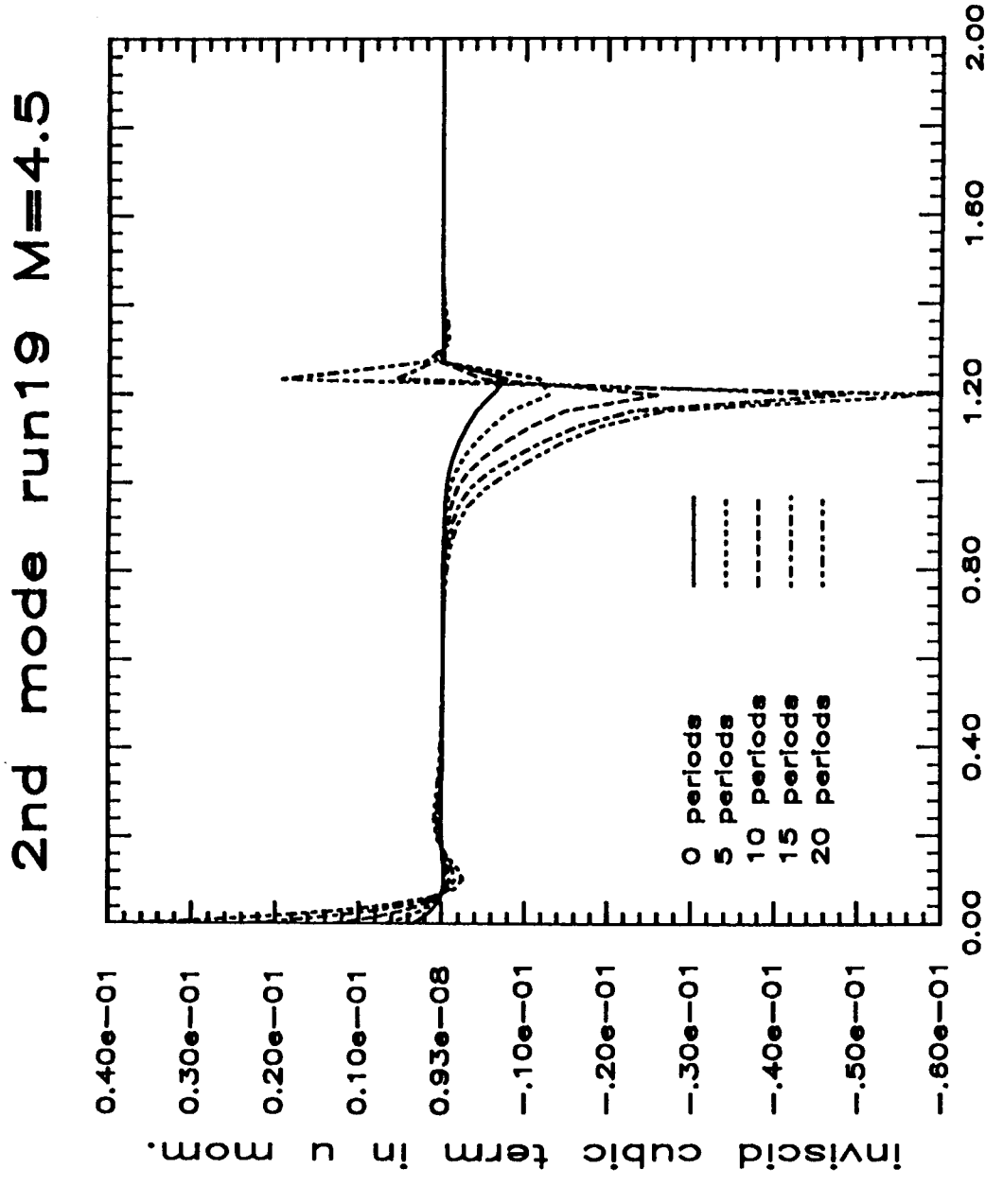
2nd mode run19 M=4.5
inviscid cubic term in u mom.
0.40e-01
0.30e-01
0.20e-01
0.10e-01
0.93e-08
-.10e-01
-.20e-01
-.30e-01
-.40e-01
-.50e-01
-.60e-01
0.00
0.40
0.80
1.20
1.60
2.00
y
0 periods
5 periods
10 periods
15 periods
20 periods

Figure 4b

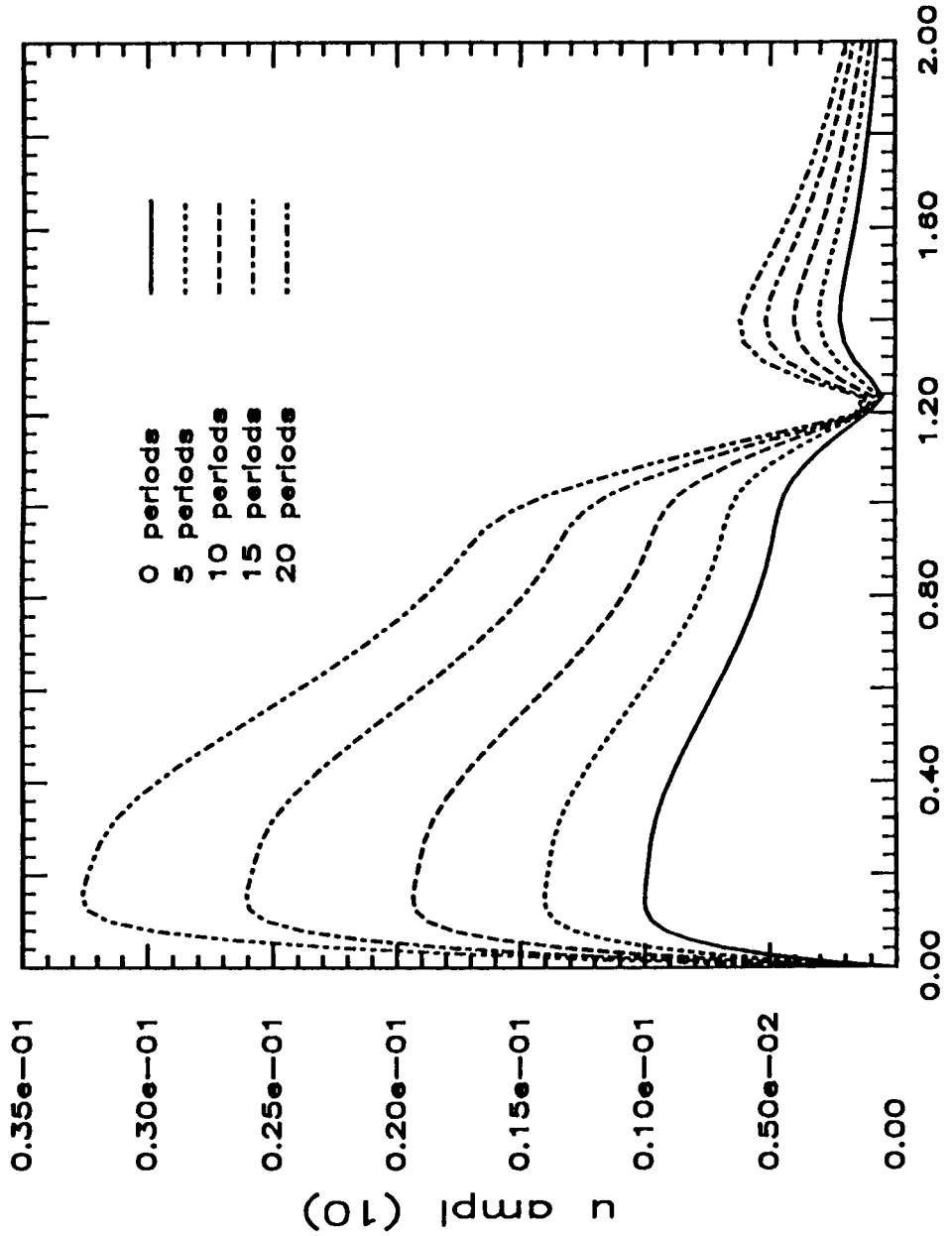
2nd mode run19 M=4.5
0 periods
5 periods
10 periods
15 periods
20 periods
u ampl (10)
0.35e-01
0.30e-01
0.25e-01
0.20e-01
0.15e-01
0.10e-01
0.50e-02
0.00
0.00
0.40
0.80
1.20
1.60
2.00
y

Figure 5a

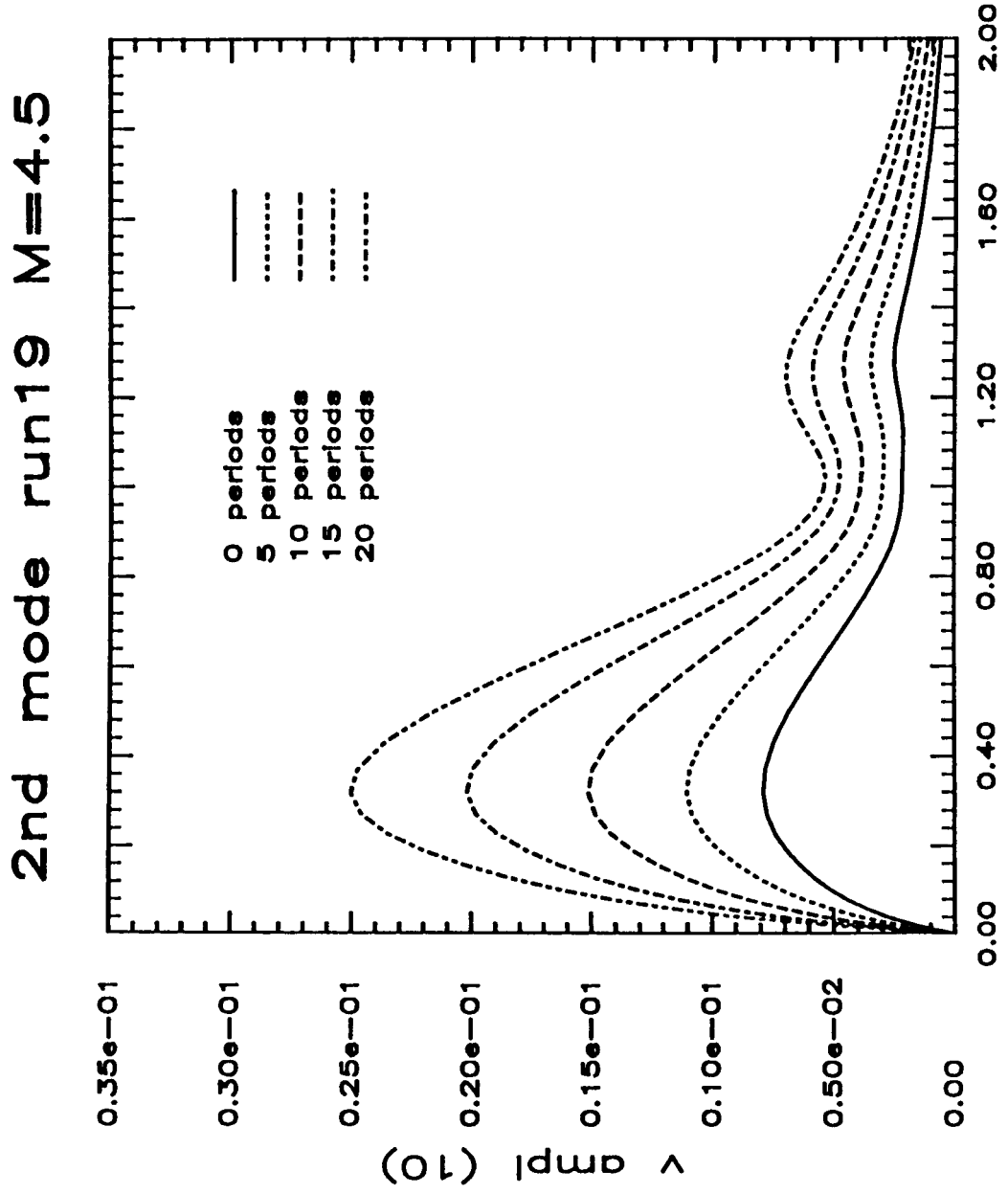
2nd mode run19 M=4.5
0 periods
5 periods
10 periods
15 periods
20 periods
v ampl (10)
0.35e-01
0.30e-01
0.25e-01
0.20e-01
0.15e-01
0.10e-01
0.50e-02
0.00
0.00
0.40
0.80
1.20
1.60
2.00
y

Figure 5b

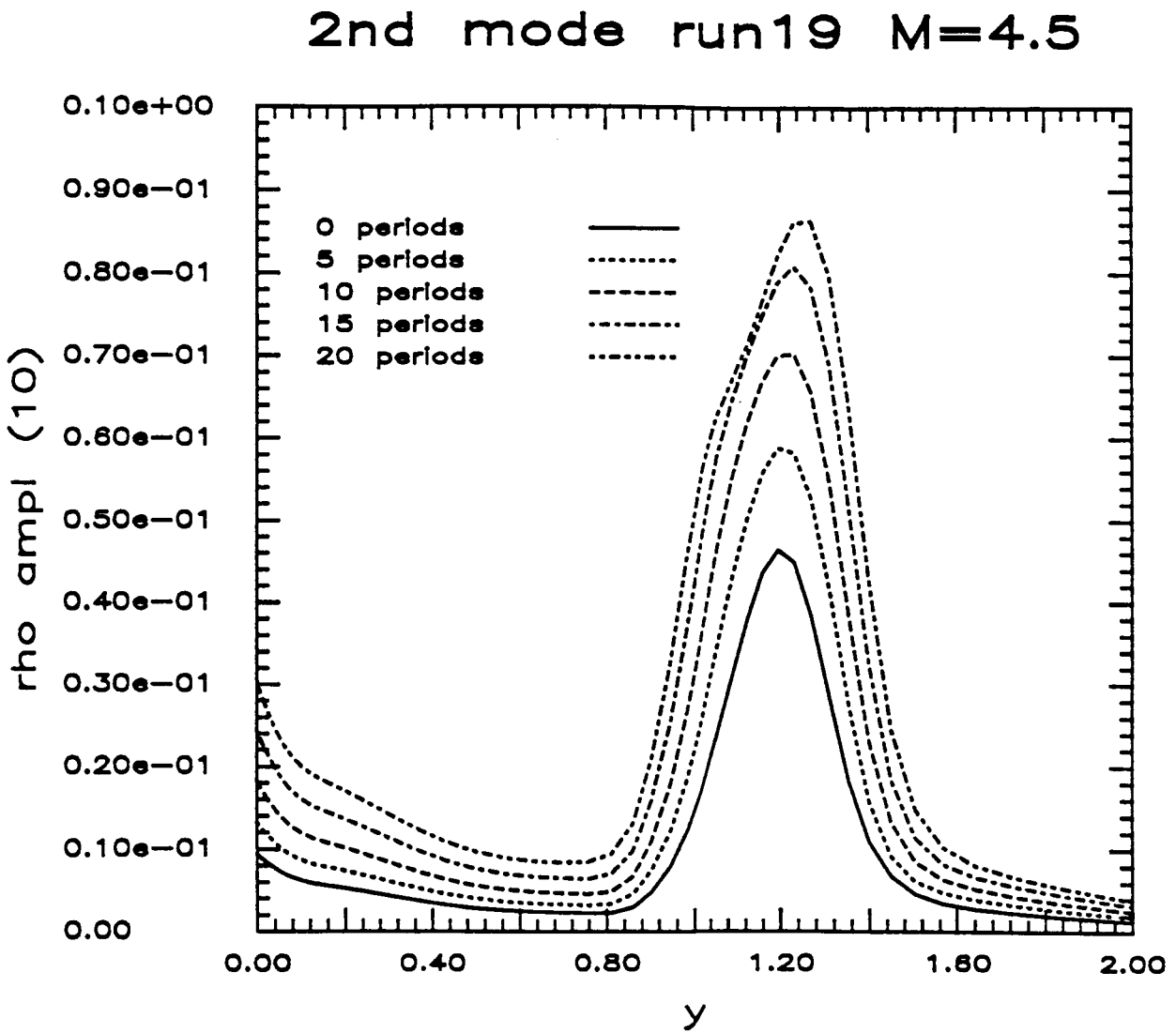
2nd mode run19 M=4.5
0.10e+00
0.90e-01
0.80e-01
0.70e-01
0.60e-01
0.50e-01
0.40e-01
0.30e-01
0.20e-01
0.10e-01
0.00
rho ampl (10)
0 periods
5 periods
10 periods
15 periods
20 periods
0.00
0.40
0.80
1.20
1.60
2.00
y

Figure 5c

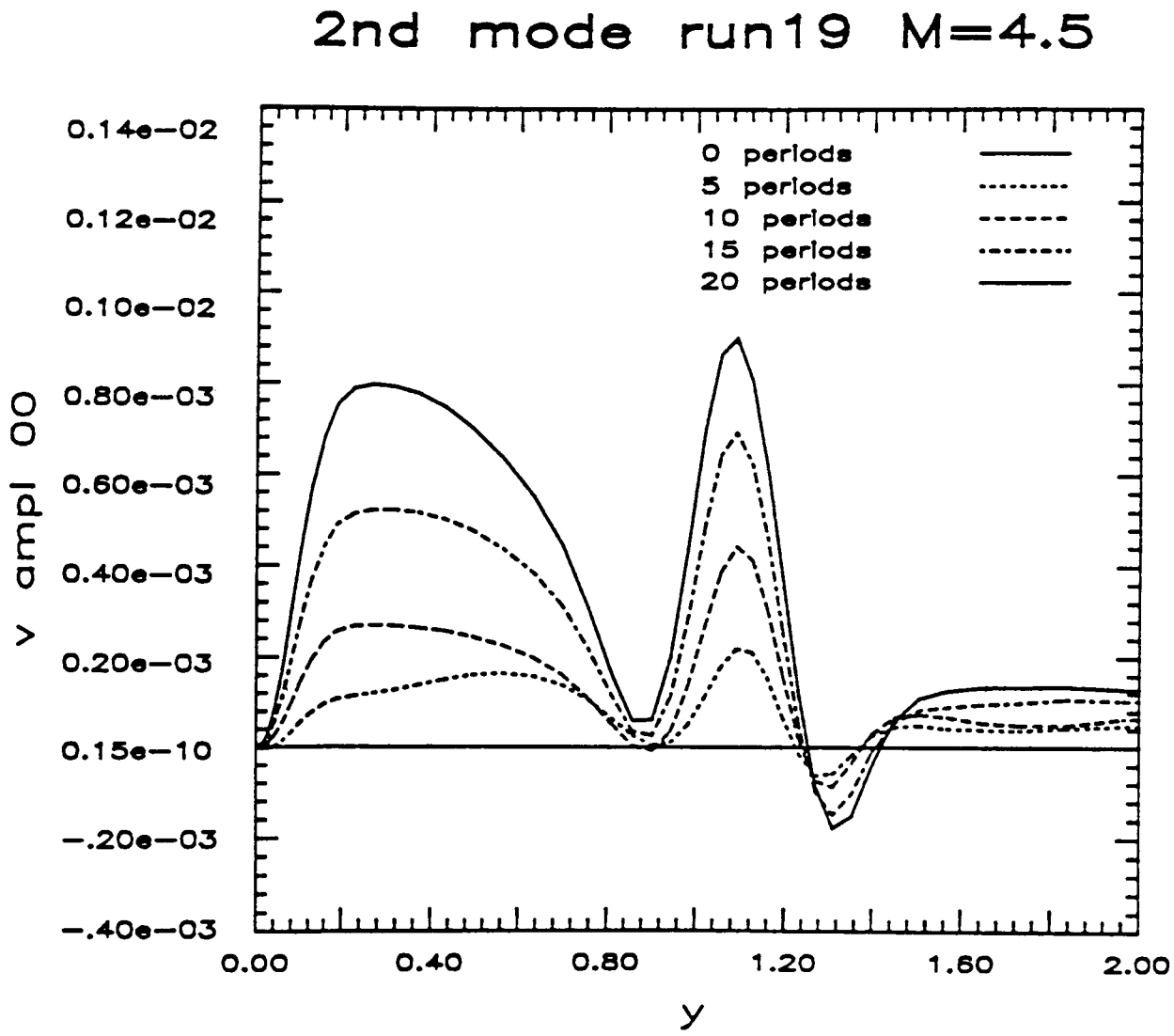
2nd mode run19 M=4.5
0.14e−02
0.12e−02
0.10e−02
0.80e−03
0.60e−03
0.40e−03
0.20e−03
0.15e−10
−.20e−03
−.40e−03
v ampl 00
0.00
0.40
0.80
1.20
1.60
2.00
y
0 periods
5 periods
10 periods
15 periods
20 periods

Figure 6

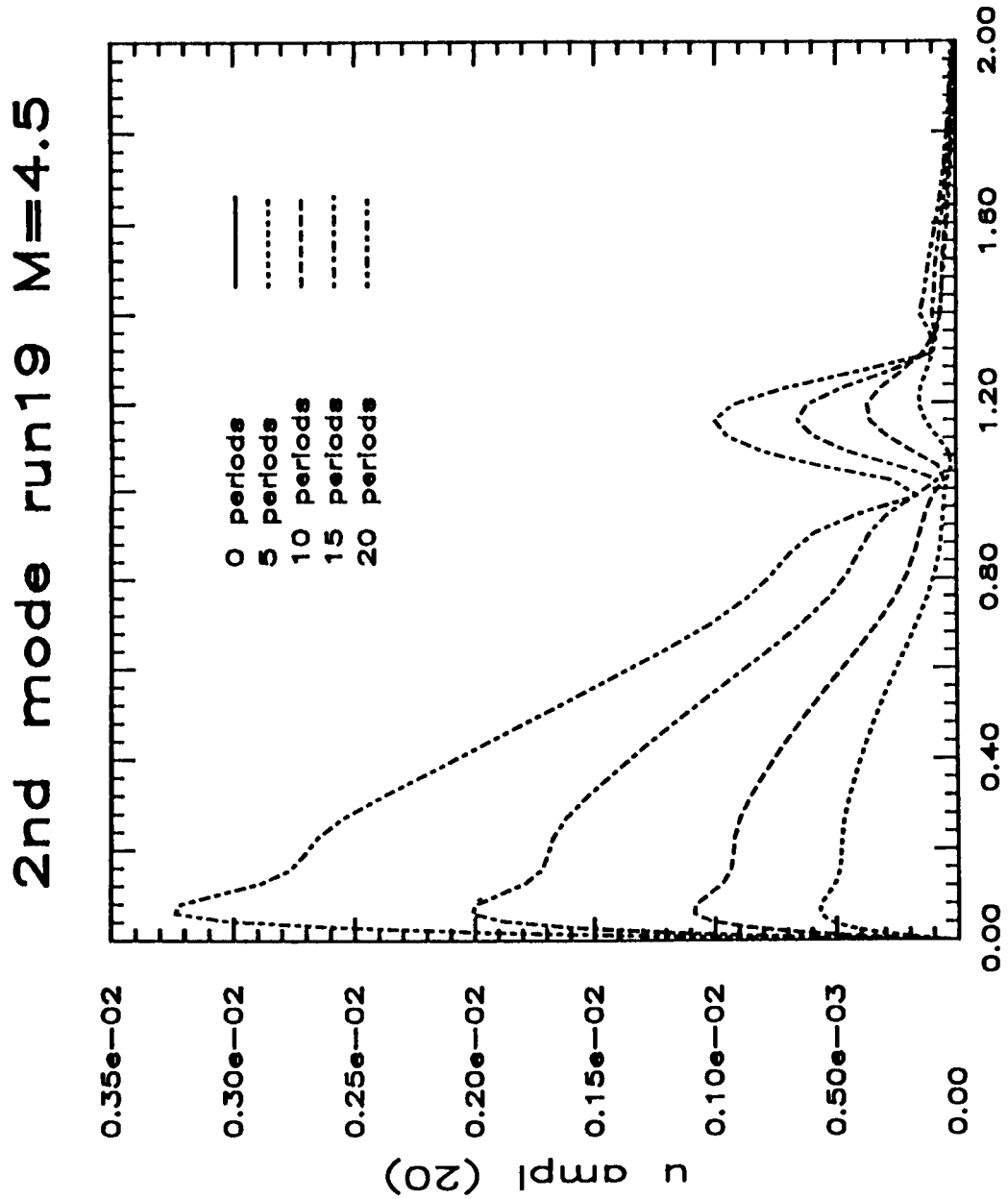
2nd mode run19 M=4.5
0 periods
5 periods
10 periods
15 periods
20 periods
u ampl (20)
0.35e-02
0.30e-02
0.25e-02
0.20e-02
0.15e-02
0.10e-02
0.50e-03
0.00
0.00
0.40
0.80
1.20
1.60
2.00
y

Figure 7a

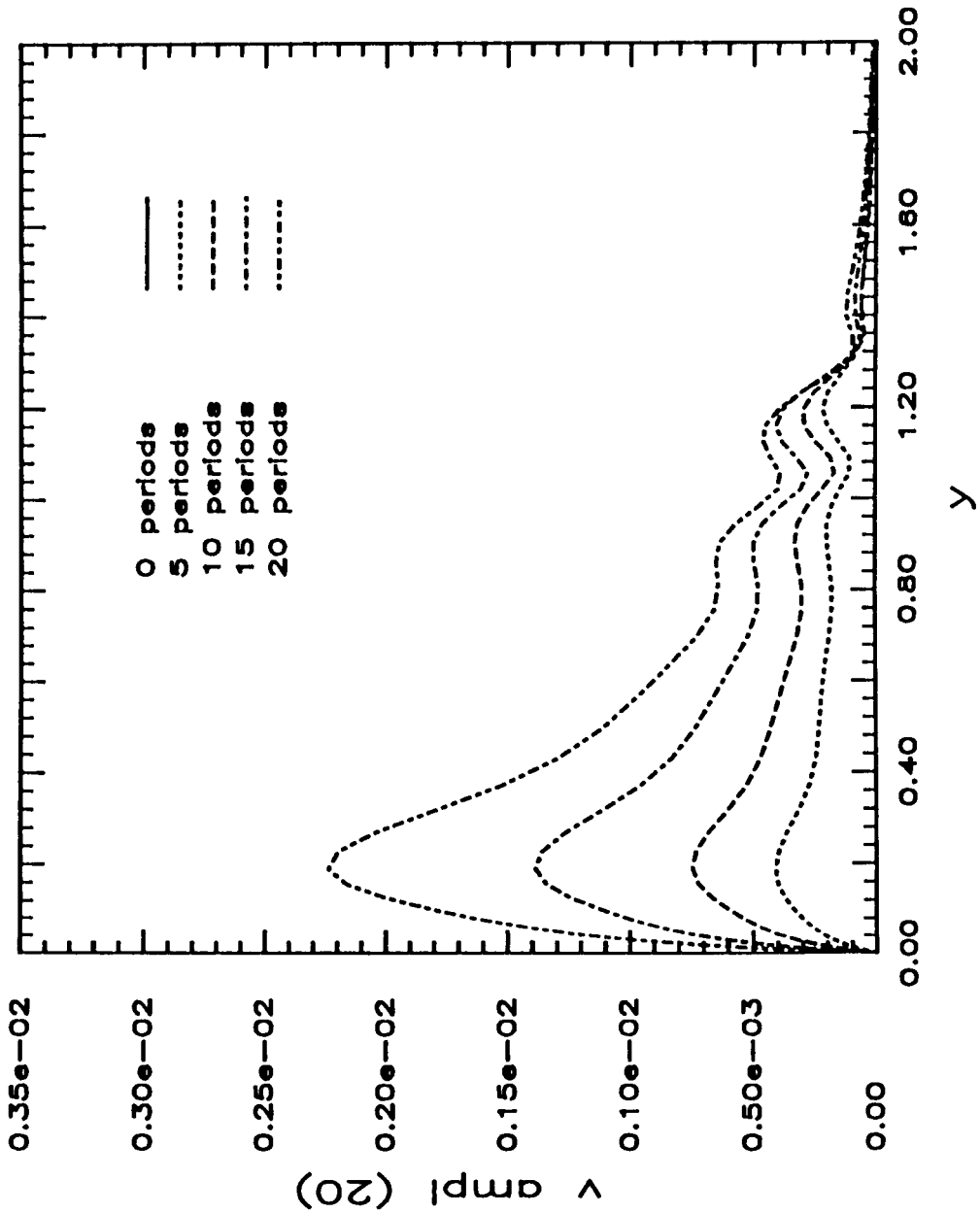
2nd mode run19 M=4.5
0 periods
5 periods
10 periods
15 periods
20 periods
v ampl (20)
0.35e-02
0.30e-02
0.25e-02
0.20e-02
0.15e-02
0.10e-02
0.50e-03
0.00
0.00
0.40
0.80
1.20
1.60
2.00
y

Figure 7b

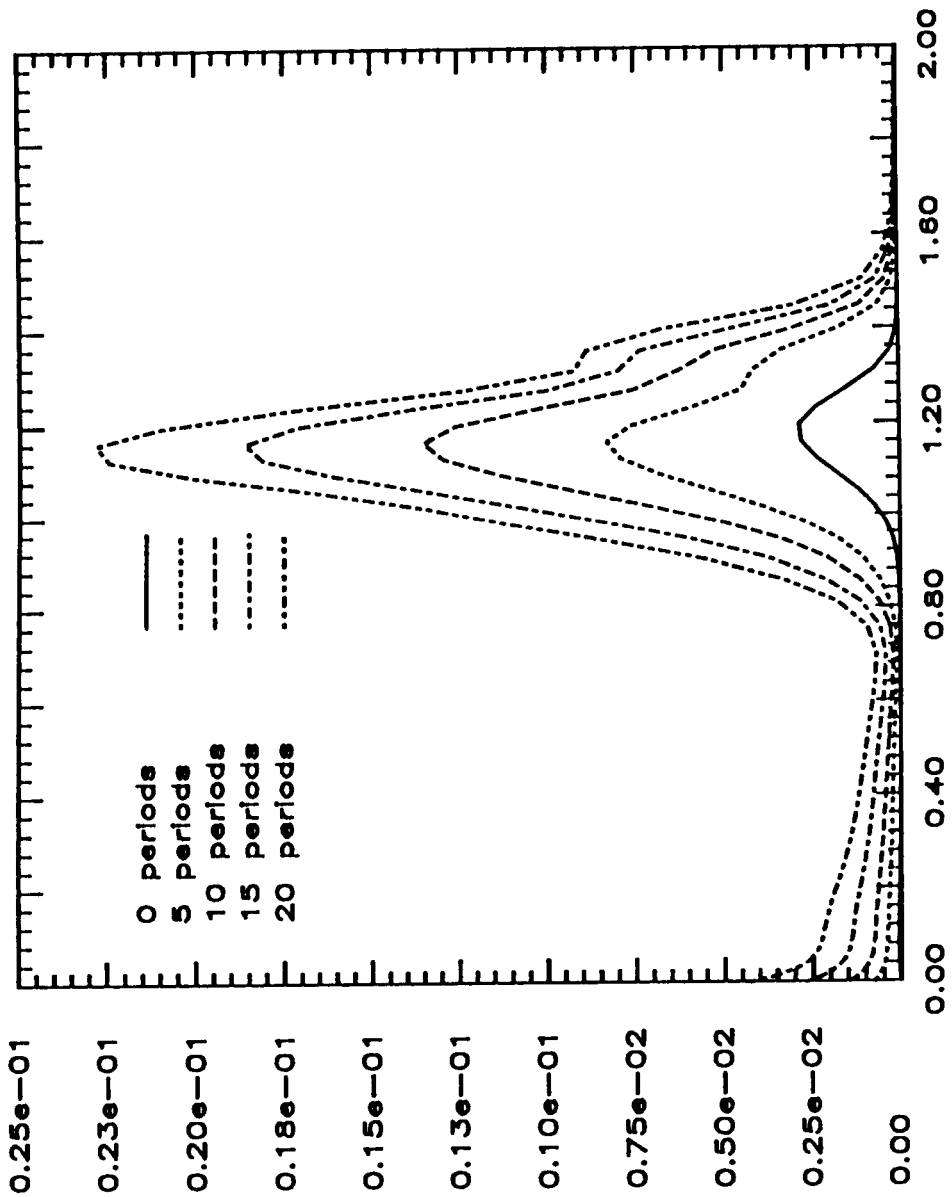
2nd mode run19 M=4.5
0 periods
5 periods
10 periods
15 periods
20 periods
rho ampl (20)
0.25e-01
0.23e-01
0.20e-01
0.18e-01
0.15e-01
0.13e-01
0.10e-01
0.75e-02
0.50e-02
0.25e-02
0.00
0.00
0.40
0.80
1.20
1.60
2.00
y

Figure 7c

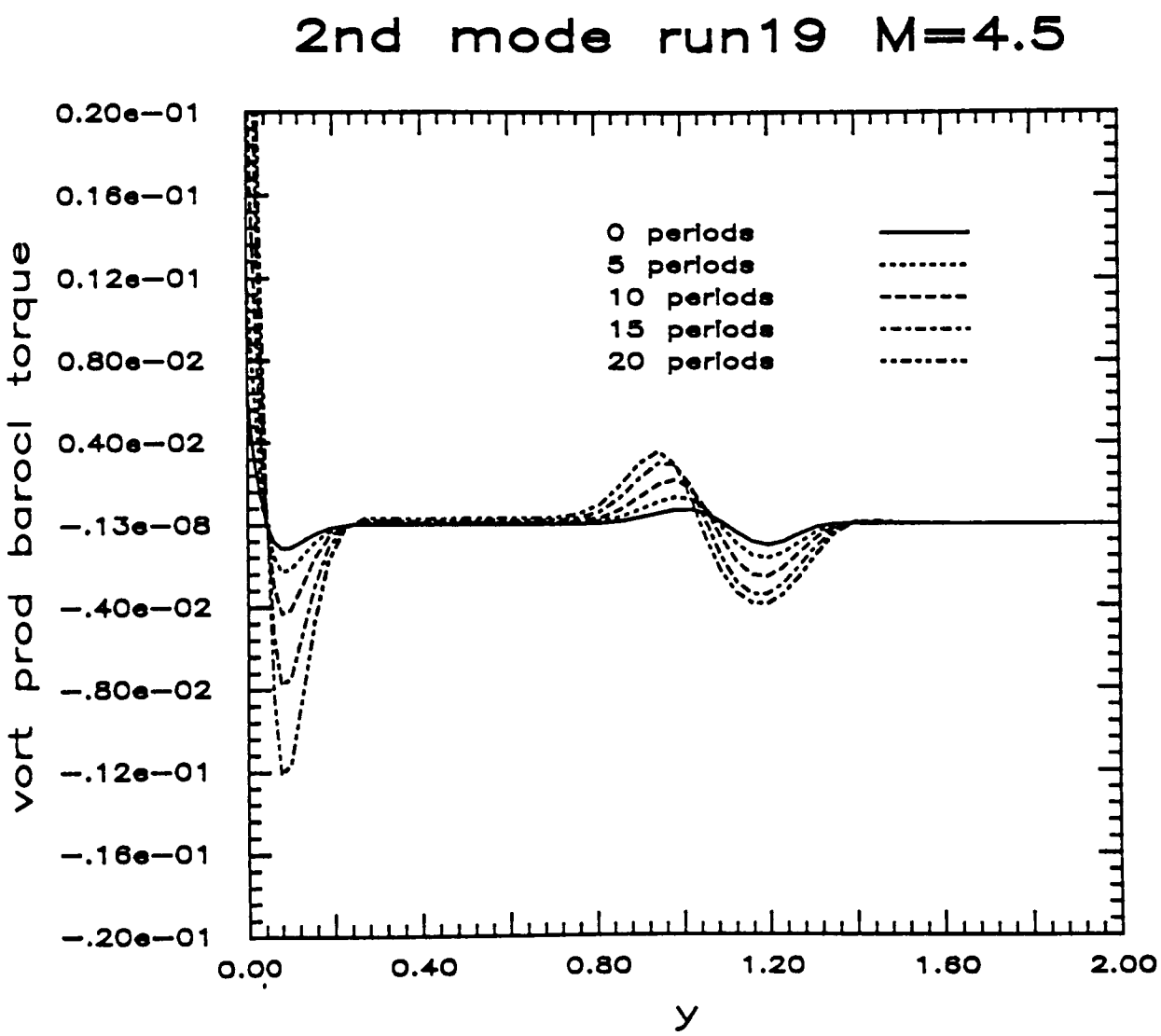
2nd mode run19 M=4.5
0.20e-01
0.16e-01
0.12e-01
0.80e-02
0.40e-02
-.13e-08
-.40e-02
-.80e-02
-.12e-01
-.16e-01
-.20e-01
vort prod barocl torque
0.00
0.40
0.80
1.20
1.60
2.00
y
0 periods
5 periods
10 periods
15 periods
20 periods

Figure 8a

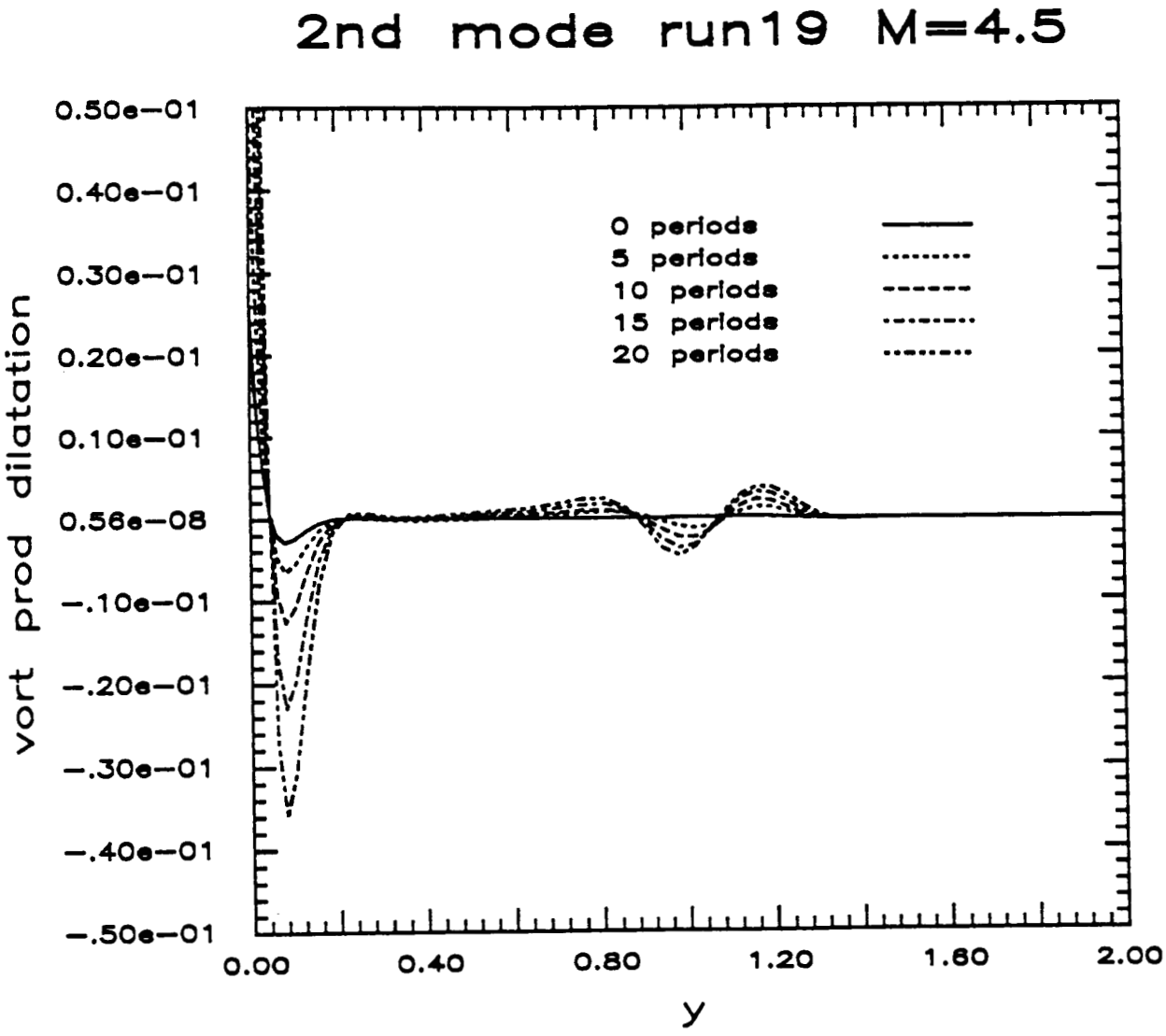
2nd mode run19 M=4.5
0.50e−01
0.40e−01
0.30e−01
0.20e−01
0.10e−01
0.56e−08
−.10e−01
−.20e−01
−.30e−01
−.40e−01
−.50e−01
vort prod dilatation
0 periods
5 periods
10 periods
15 periods
20 periods
0.00
0.40
0.80
1.20
1.60
2.00
y

Figure 8b

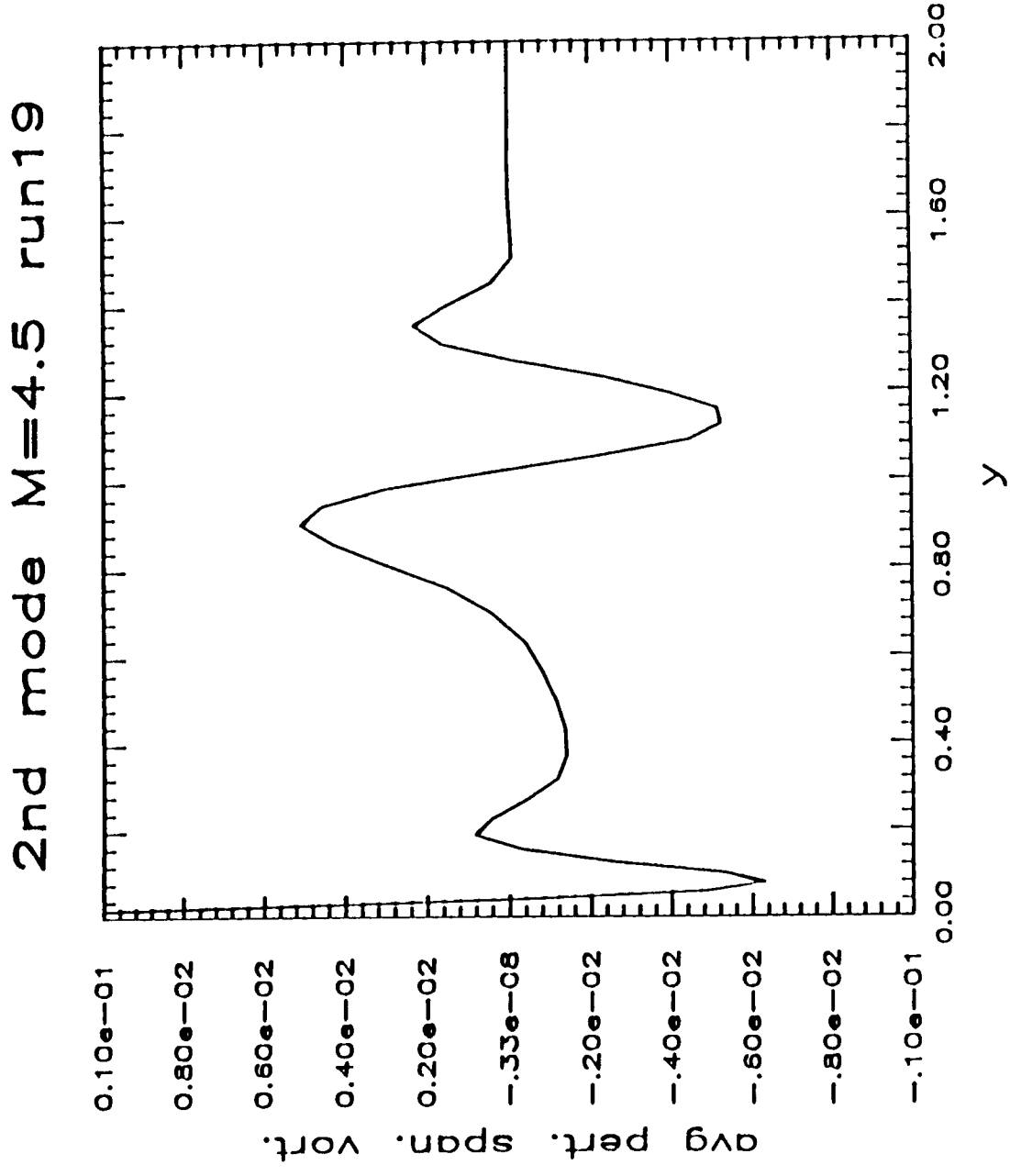
2nd mode M=4.5 run19
avg pert. span. vort.
0.10e-01
0.80e-02
0.60e-02
0.40e-02
0.20e-02
-.33e-08
-.20e-02
-.40e-02
-.60e-02
-.80e-02
-.10e-01
0.00
0.40
0.80
1.20
1.60
2.00
y

Figure 9

NASA
National Aeronautics and Space Administration

Report Documentation Page

1. Report No.	2. Government Accession No.	3. Recipient's Catalog No.
NASA CR-181811 ICASE Report No. 89-15		

4. Title and Subtitle

NON-LINEAR EVOLUTION OF A SECOND MODE WAVE IN SUPERSONIC BOUNDARY LAYERS

5. Report Date

February 1989

6. Performing Organization Code

7. Author(s)

Gordon Erlebacher
M. Y. Hussaini

8. Performing Organization Report No.

89-15

10. Work Unit No.

505-90-21-01

9. Performing Organization Name and Address

Institute for Computer Applications in Science and Engineering
Mail Stop 132C, NASA Langley Research Center
Hampton, VA 23665-5225

11. Contract or Grant No.

NAS1-18605

13. Type of Report and Period Covered

Contractor Report

12. Sponsoring Agency Name and Address

National Aeronautics and Space Administration
Langley Research Center
Hampton, VA 23665-5225

14. Sponsoring Agency Code

15. Supplementary Notes

Langley Technical Monitor:
Richard W. Barnwell

Final Report

Applied Numerical Mathematics

16. Abstract

The non-linear time evolution of a second mode instability in a Mach 4.5 wall-bounded flow is computed by solving the full compressible, time-dependent Navier-Stokes equations. High accuracy is achieved by using a Fourier-Chebyshev collocation algorithm. Primarily inviscid in nature, second modes are characterized by high frequency and high growth rates compared to first modes. Time evolution of growth rate as a function of distance from the plate suggests this problem is amenable to the Stuart-Watson perturbation theory as generalized by Herbert.

17. Key Words (Suggested by Author(s))	18. Distribution Statement
compressible boundary layers, transition, stability	34 - Fluid Mechanics & Heat Transfer Unclassified - Unlimited

19. Security Classif. (of this report)	20. Security Classif. (of this page)	21. No. of pages	22. Price
Unclassified	Unclassified	39	A03

NASA FORM 1626 OCT 86